DEBRE BERHAN UNIVERSITY

COLLEGE OF NATURAL AND COMPUTATION SCIENCE

DEPARTMENT OF CHEMISTRY

Synthesis of g-C_3N_4/$CoFe_2O_4$ Composite for Photocatalytic Degradation of Methylene blue in Aqueous Solution

By: Tesfa Mengist

Advisor: Hulugergish Degefu (PhD)

February 2021

Debre Berhan, Ethiopia

DEBRE BERHAN UNIVERSITY
POSTGRADUATE STUDIES
COLLEGE OF NATURAL AND COMPUTATIONAL SCIENCES

Synthesis of g-C_3N_4/$CoFe_2O_4$ Composite for Photocatalytic Degradation of Methylene Blue in Aqueous Solution

By: Tesfa Mengist

Advisor: Hulugergish Degefu (PhD)

A Thesis Submitted to Debre Berhan University Department of Chemistry in the Partial Fulfillment of Master of Science in Chemistry

Feburary 2021

Debre Berhan, Ethiopia

DEBRE BERHAN UNIVERSITY
POSTGRADUATE STUDIES
COLLEGE OF NATURAL AND COMPUTATIONAL SCIENCES

APPROVAL SHEET I

This is to certify that the thesis entitled "**synthesis of g-C_3N_4/$CoFe_2O_4$ using chemical co-precipitation method for photocatalytic degradation of methylene blue in aqueous solution**" submitted in partial fulfillment of requirements Degree of Master of Science in Chemistry, College of Natural and Computational Science, Debre Berhan University and is a faithful record of original research work carried out by Tesfa Mengist kibrete under my guidance and supervision. No part of this thesis has been submitted for any other degree or diploma.

It is further certified that the assistance and help received by him from various sources during the course of investigation have been duly acknowledged. Therefore, I recommend that it be accepted as fulfilling the thesis requirements.

Hulugergish Degefu (PhD)	_____	_____
Major Advisor	Signature	Date

DEBRE BERHAN UNIVERSITY

COLLEGE OF GRADUATE STUDIES

COLLEGE OF NATURAL AND COMPUTATIONAL SCIENCES

APPROVAL SHEET II

We, the undersigned members of the boarded of the examiners of the final open defense by Tesfa Mengist have read and evaluated his thesis entitled "**synthesis of g-C_3N_4/$CoFe_2O_4$ using chemical co-precipitation method for Photocatalytic degradation of methylene blue in aqueous solution**" and examined the candidates. This is, therefore, to certify that the thesis has been accepted in partial fulfillment of the requirements for the degree of Masters of Science in chemistry.

Hulugergish Degefu (PhD)	_____	_____
Major Advisor	Signature	Date
_____	_____	_____
Name of external examiner	Signature	Date
_____	_____	_____
Name of internal examiner	Signature	Date
_____	_____	_____
Name of chairman	Signature	Date

STATEMENT OF THE AUTHOR

I declare that this thesis is my original work and that all sources of materials used for this thesis have been duly acknowledged. This thesis had been submitted in partial fulfillment of the requirements for MSc degree in chemistry to Debre Berhan University at College of Natural and Computational Sciences and has been carried out by me at the Department of chemistry, Debre Berhan University, Debre Berhan, Ethiopia, under the supervision of Dr. Hulugergish Degefu. It is made available at the University's Library to borrowers under rules and regulations of the Library. I solemnly declare that this thesis is not submitted to any other institution anywhere for the award of any academic degree, diploma or certificate.

Brief quotations from this thesis are allowed without prior and /or special permission provided that due acknowledgment of the source is properly made in all other instances; however, permission must be obtained from the author.

Name: Tesfa Mengist Signature _____

Place: Debre Berhan University

Department: Chemistry

Date of Submission: _____

ACKNOWLEDGMENTS

First and foremost, I would like to thank God for all the blessing and gave me strength and wisdom to accomplish this research work. I am deeply grateful my sincere appreciation to my supervisor, Dr. Hulugergish Degefu, Assistance professor of physical Chemistry for providing me the great opportunity to carry out this project. I am deeply grateful for her continuous support, instructive advice and encouragement. I would also like to express my deepest gratitude to D.r Newaye Belachew (Assistance professor of Inorganic and Nanochemistry) and Hirpo Hinsene (MSc, Analytical chemistry) for directed me during lab work and thesis writing. I acknowledge the Debre Berhan University Chemistry Department to facilitate laboratory instruments and equipment. I am also grateful to extend my gratitude to the department head of Chemistry for his genuine encouragement and material support given whenever it was available. Last but not the least, I would like to thank my Family and Friends who always believe in me and support in all my decisions.

ABSTRACT

Herein, in this study, we have reported a successful synthesis of g-C_3N_4, $CoFe_2O_4$ Nps and g-C_3N_4/$CoFe_2O_4$ nanocomposite materials for photocatalytic degradation of methylene blue dye. Direct calcination of urea at 550 ^oC for 3 h was employed to synthesize g-C_3N_4, $CoFe_2O_4$ and synthesized using a facile co- precipitation method. Besides, g-C_3N_4/$CoFe_2O_4$ nanocomposite was synthesized by a simple co-precipitation method. The crystalline structure, functional group presents and surface charge of the synthesized photo catalysts was investigated by powder XRD, FTIR and pH_{pzc} techniques respectively. The XRD analyses show the formation of the desired phases of g-C_3N_4, $CoFe_2O_4$ NPs and g-C_3N_4/$CoFe_2O_4$ composites. The photocatalytic efficiency of the synthesized semiconductor materials were investigated by the degradation of MB. Among the synthesized nonmaterial's, g-C_3N_4/$CoFe_2O_4$ shows maximum photocatalytic efficiency than the other which is due to lowering the band gap and effectively reduces the recombination rate of electron-hole pairs during the photocatalytic reaction. The photocatalytic activities were investigated at varying pH of solution, contact time (min), initial concentration of MB (mg/L), and photocatalyst dose (mg).

Keywords: Photocatalysis, Methylene blue degradation, g-C_3N_4, $CoFe_2O_4$, g-C_3N_4/$CoFe_2O_4$

Acronyms and Abbreviations

COD	Crystal Open Data base
FTIR	Fourier Transform Infrared Spectroscopy
g-C_3N_4	Graphitic Carbon Nitride
JCPDS	Joint Committee on Powder Diffraction Standards
MB	Methylene Blue
M	Molar
NP	Nanoparticles
PHpzc	Point Zero Charge
PPM	Parts Per Million
PXRD	Powder X-ray Diffraction
Uv-Vis	Ultraviolet-Visible

TABLE OF CONTENTES

LIST OF CONTENTS Page

LIST OF TABLES

TABLE OF CONTENTS Page

LIST OF FIGURES

Figure of Contents Page

CHAPTER ONE

1. INTRODUCTION

1.1 Background of the Study

Water is not only fundamental to our life and health but also essential for all life on the earth without any substitute [1]. Recently, a growing population with increasing standard of human beings' living, food production and industrialization has been putting much pressure on the water resource [2]. Pollutions and contaminations have been turning the limited fresh water into wastewater [3]. Although saving water is a matter for easing water problems, water is still limited globally; therefore, wastewater treatment seems increasingly important when more and more sewage is discharged from industries and households [4]. Manufacturers including the textile industry utilize thousands of types of dyes and pigments, generating a large amount of wastewater containing dyes, which must be treated before released. Currently, there are mainly three means to treat dye-polluted water: the chemical, physical and biological methods [5].

Photocatalytic degradation of dyes or other organic pollutants is an intensively pursued research exercise mainly from the last quarter half of the 20^{th} century [6]. Nowadays, the synthetic dyes are extensively used in products like clothes, leather accessories, furniture, and plastic products. However, during the dyeing process, nearly 12% of these dyes exclude as waste, and ~ 20% of this wastage enters to the environment [7]. In the dye degradation process, large molecules of dyes get oxidized down into smaller molecules such as water, carbon dioxide, and other mineral byproducts. As stated, the dyeing process does not utilize all the dye molecules, and consequently, a substantial amount of dyes were present in the waste water released from the industry [8].

The heterogeneous photocatalysis eliminating an organic pollutant from water or air has numerous potential applications [9] to resolve serious environmental pollution. In recent years, researchers have devoted extensive efforts to prepare semiconductors for the photocatalytic reaction with a suitable band gap, such as metal-containing oxide, sulfide, and oxynitride. Very recently, a novel metal-free semiconductor photocatalyst, carbon nitride (C_3N_4), was found to have good performance in the photo oxidation of methyl orange (MO), the developed g-C_3N_4metal including compounds could effectively degrade MO dyes. Wanget al. also reported

that g-$C_3N_4$with a band gap of 2.7eV achieved functionality as a stable photocatalyst for H_2evolution from water under visible light irradiation [10].

Covalent carbon nitrides have attracted much attention since the theoretical prediction of their remarkable mechanical and electronic properties of some phases [11], for example, g-$C_3N_4$was used as catalyst or carrier due to its excellent stability at an ambient condition [11]. In most cases, g-C_3N_4 powder was prepared by a facile pyrolysis method using amine precursors [10]. However, the obtained g-$C_3N_4$from varying amine precursors may present the discrepant photocatalytic properties. To develop a highly efficient photocatalytic system, it is interesting to know the photocatalytic properties of g-C_3N_4depending on the precursors. The detailed investigations on g-C_3N_4will provide useful information for its photocatalysis application. Here, the g-C_3N_4powder was prepared by heating cyanamide, dicyandiamide, and melamine, respectively, and the photocatalytic activity was evaluated by the photo degradation of methylene blue (MB). The results suggest that the obtained g-C_3N_4 presented the distinct performance of photocatalysis, which depended on the amine precursor.

Graphite-like C_3N_4 (g-C_3N_4) is an all-organic delocalized π conjugative structured material with band gap of ~2.7 eV, which could be used as high performance photocatalyst under visible-light. In addition, due to the delocalized π-π structure, -induced charge g-C_3N_4 also possesses rapid photo-induced charge separation and relatively slow charge recombination property in the electron transfer process [12]. Meanwhile, the g-C_3N_4 is regarded as the most stable allotrope among the carbon nitride materials under ambient conditions as well as in high acid or base solutions due to the strong covalent bonds between carbon and nitride atoms [13]. Therefore, the modification of g-C_3N_4 could give rise to nanocomposites with visible-light activity, better charge separation and relatively slow charge recombination and enhanced photo or chemical stability [14].However, nanostructure g-C_3N_4 and bulk g-C_3N_4 both face another problem, which is difficult to be separated after the photocatalytic reaction.

An efficient and facile way to separate the catalyst from the suspension is to combine g-$C_3N_4$with a magnetic material [15].

As a part of the ferrite family, magnetic $CoFe_2O_4$ spinel is in the focus of research because of its potential use in various applications. Due to its magnetic properties, $CoFe_2O_4$ nanoparticles may

be employed in catalysts , cathode electro catalyst of microbial fuel cells , or in various functional composite materials , including advanced adsorbents, for the removal of anionic pollutants from water [16]. Ferrites are magnetic ceramics of great importance in countless scientific and technological applications on account of their numerous electrical, magnetic, and dielectric properties. In the class of ferrites, spinel ferrites with chemical formula MFe_2O_4 (where, M represents divalent ions of the transition metal elements such as Co^{2+}, Ni^{2+}, Zn^{2+}, Mg^{2+}, etc.) are industrially leading magnetic materials due to their outstanding electromagnetic properties [17].

Transition metal ferrites can be more appropriate and promising due to the several advantages like, it is an effective catalyst with specific active sites and most importantly its narrow band gap matches with the solar spectrum [18]. Among the various semiconducting ferrite materials $CoFe_2O_4$ with spinel structure is more promising due to its narrow band gap, good photochemical stability, favorable magnetic property and it can exhibit characteristic photochemical the visible-light irradiation [19]. Spinel $CoFe_2O_4$ has several features, such as high electro-magnetic performance, excellent chemical stability, remarkable mechanical hardness and ferromagnetic behaviors [20].

A composite material is a material fabricated from two or more constituent materials with considerably different physical or chemical properties that, once combined, produce a material with characteristics different from the parent source materials [21]. Recently, numerous researches have been made to couple g-C_3N_4 with various semiconductors to enhance the photocatalytic activities. For instances, Wang and co-workers firstly reported TiN/g-C_3N_4 multi-layers hybridization by using a dual facing-target magnetron sputtering method at room temperature, an exhibited favorable properties in photocatalytic applications.

Above all, as a magnetic material, $CoFe_2O_4$ has emerged a great advantage in the application of degrading organic pollutants. Besides, it has been reported that g-C_3N_4could activate H_2O_2 to degrade organic pollutants under visible light irradiation [22]. Therefore, the combination of $CoFe_2O_4$ and g-C_3N_4 could be beneficial, since it would fabricate an efficient, stable and magnetic photocatalyst to activate H_2O_2 for removing organic pollutants [23].

1.2 Statement of the Problem

Water pollution is the contamination of water bodies such as lakes, rivers, oceans, and groundwater caused by either human activities or industrial activities, which can be harmful to organisms and plants which live in these water bodies. It has always been a major problem to the environment. With industrialization in major areas and an urban city growing the water around them just keeps getting polluted. A lot of water pollution is caused by industries near rivers and lakes doing illegal dumping [24].

Our world has been faced with serious of water pollution that are discharged from numerous industries. These pollutants are introduced into the environment without being treated are responsible for bringing toxicity to the aquatic life and human. Removal of industrial wastewaters that contains both organic and inorganic pollutants are a very challenging task because it requires the use of special techniques and reaction conditions. Currently, a massive discharge of MB from different industries to water bodies is observed without being treated. Hence, in order to save the environment and human health, removal of MB from aqueous solution has taken a huge research interest. During the last decades the ever increasing of toxic discharges (pollutants) from textile, and plastics industries takes a huge responsibility for pollution of the environment [25]. Textiles industries are suspect to introduce MB to the environment. Therefore, it is desirable for removal of these toxic pollutants before releasing to the environment. In this regard, searching of low cost, environmentally friendly, and efficient water treatment methods have taken huge concern for the scientific community. A broad-spectrum degradation efficiency of the advanced oxidation process, in particular photocatalysis, has brought a promising for remediation of wastewater. Metal oxide semiconductors, such as ZnO and TiO_2, are widely employed for this purpose. However, the low photocatalytic efficiency of these semiconductors due to wide band gap energy and fast electron hole pair recombination remains a challenge for practical use. Hence, doping or make composite with other are common strategies to overcome the mentioned problems. Hence, in this study, we have introduced magnetically separable and visible light active, g-C_3N_4/$CoFe_2O_4$ composite for photocatalytic degradation of MB dye.

1.3 Objectives of the Study

1.3.1 General Objectives

The general objective of the study was:

- To synthesize g-C_3N_4/$CoFe_2O_4$ composite for photocatalytic degradation of methylene blue.

1.3.2 Specific Objectives

The specific objectives of the study were:

- ✓ To synthesize graphitic carbon nitride (g-C_3N_4) from nitrogen rich urea by pyrolysis method
- ✓ To synthesize magnetic $CoFe_2O_4$ using co-precipitation method
- ✓ To investigate the formation, crystal structure and surface functionalities of the as synthesized nanostructured material using powder XRD, FTIR and point of zero charge analysis
- ✓ To examine the photocatalytic degradation of MB blue dye

1.4 Significance of the Study

The importance of the study is:

- ✓ It will be important to apply the synthesized composite material as photocatalytic degradation of organic dye
- ✓ Researchers have used the result from this study for further investigation to overcome the industrial pollution (pollution in the country)

CHAPTER TWO

2. REVIEW OF RELATED LITERATURE

2.1 Photocatalysis

Photocatalysis refers to a phenomenon in which a substance (the catalyst) speed up a kinetically slow reaction and the catalyst is fully restored at the end of each catalytic cycle and the "Photo catalysis" is defined as a specific process for the acceleration of the "photoreaction" in the presence of a catalyst. Photocatalysis can also be regarded as the catalysis of photochemical reaction on a solid substrate, mostly a semiconductor [26].

The term "Photocatalysis" is still an arguable subject due to controversies, according to some researchers the "light" acts as a catalyst, while it always acts as a "reactant" where it is spent in the chemical process. The word" photoreaction" is sometimes explained as a "Photoinduced" or "Photoactivated," process, whereas in the field of photocatalysis, "catalytic activity" is the ability of a catalyst to show performance under light depending upon the reaction sites/active sites at the catalyst.

The performance of a catalyst can be determined by its "turnover frequency" which is "number of turnovers per unit time of reaction, it is used to show how many times one active site produces a reaction product(s) within unit time." In case of photocatalysis, the reaction rate depends on the frequency of irradiated light which acts as the initiator of photoreaction. The term photocatalysis indicates the relation of light and some substance; (say a catalyst) so in the absence of light, the process of photo catalytic activities on active sites is not possible [27].

2.2 Photocatalytic Mechanism

Photocatalytic reaction primarily depends on wavelength or light (photon) energy and the catalyst. In general, semiconducting materials are used as a catalyst which performs as sensitizers for the irradiation of light stimulated redox process due to their electronic structure, which is characterized by a filled valence band and a vacant conduction band [28]. Figure 2.1 shows the schematic representation of semiconductor photocatalytic mechanism. The fundamental steps in the process of semiconductor photocatalysis are as follows [29].

- When the light energy in terms of photons fall on the surface of a semiconductor and if the energy of incident ray is equivalent or more than the band gap energy of the semiconductor, the valence band electrons are agitated and move to the conduction band of the semiconductor.

.

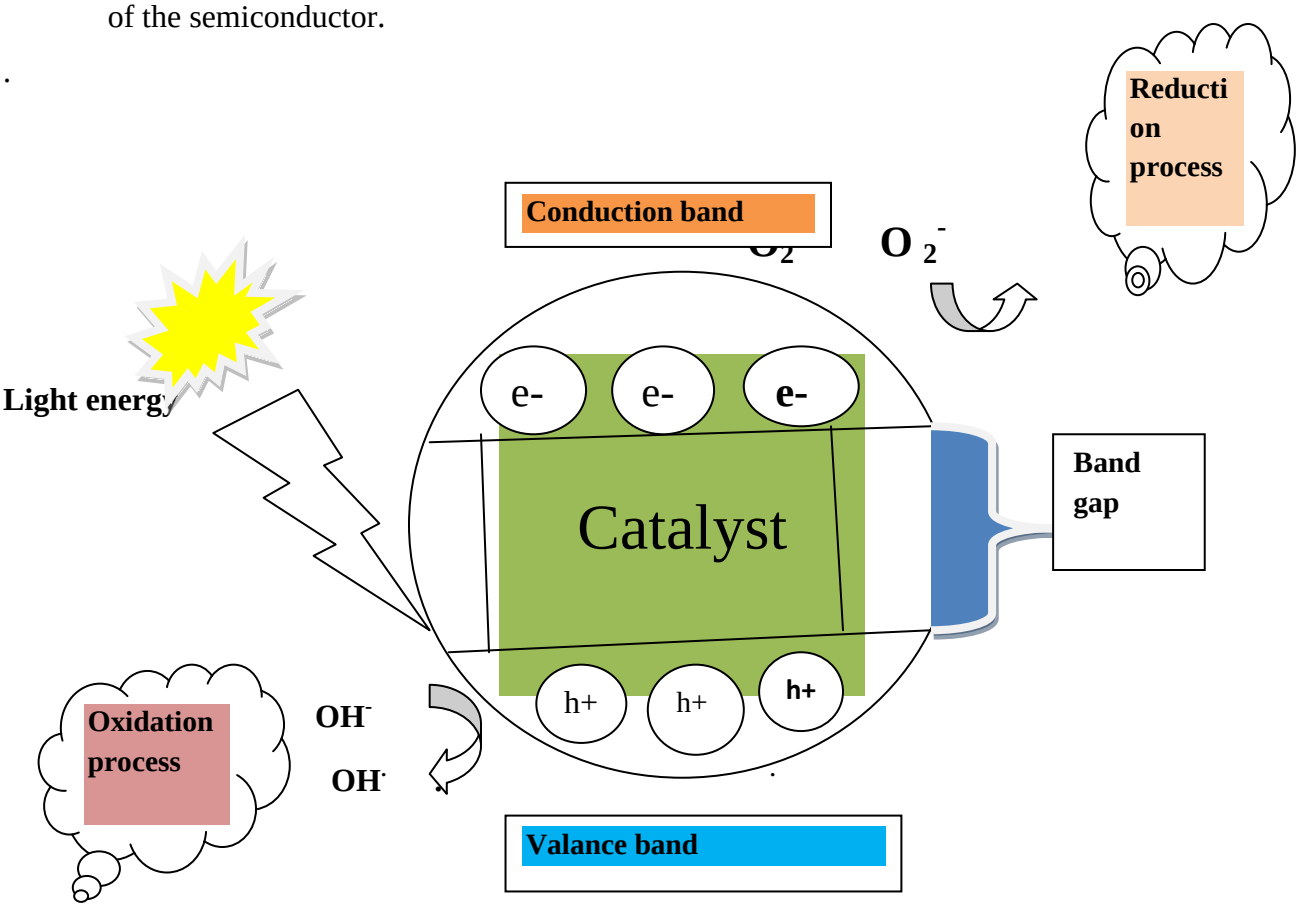

Figure2.1Schematic representation of semiconductor photocatalytic mechanism [30]

- Holes would be left in the valence band of the semiconductor. These holes in the valence band can Oxidize donor molecules and react with water molecules to generate hydroxyl radicals (The hydroxyl Radical have strong oxidizing power responsible for the degradation of pollutants).
- The conduction band electrons react with dissolved oxygen species to form superoxide ions. These electrons induce the redox reactions. These holes and electrons could undergo successive oxidation and reduction reactions with any species, which might be adsorbed on the surface of the semiconductor to give the necessary products.

2.2.1 Description of Oxidation Mechanism

The photocatalyst surface contains water, which is mentioned as “absorbed water.” This water is oxidized by positive holes created in the valence band due to the electrons shift to the conduction band as a result of light irradiation, thus making way for the formation of hydroxyl (OH·) radicals (agents which have strong oxidative decomposing power). Afterward, these hydroxyl radicals react with organic matter present in the dyes. If oxygen is present when this process happens, the intermediate radicals in the organic compounds along with the oxygen molecule can experience radical chain reactions and consume oxygen in some cases

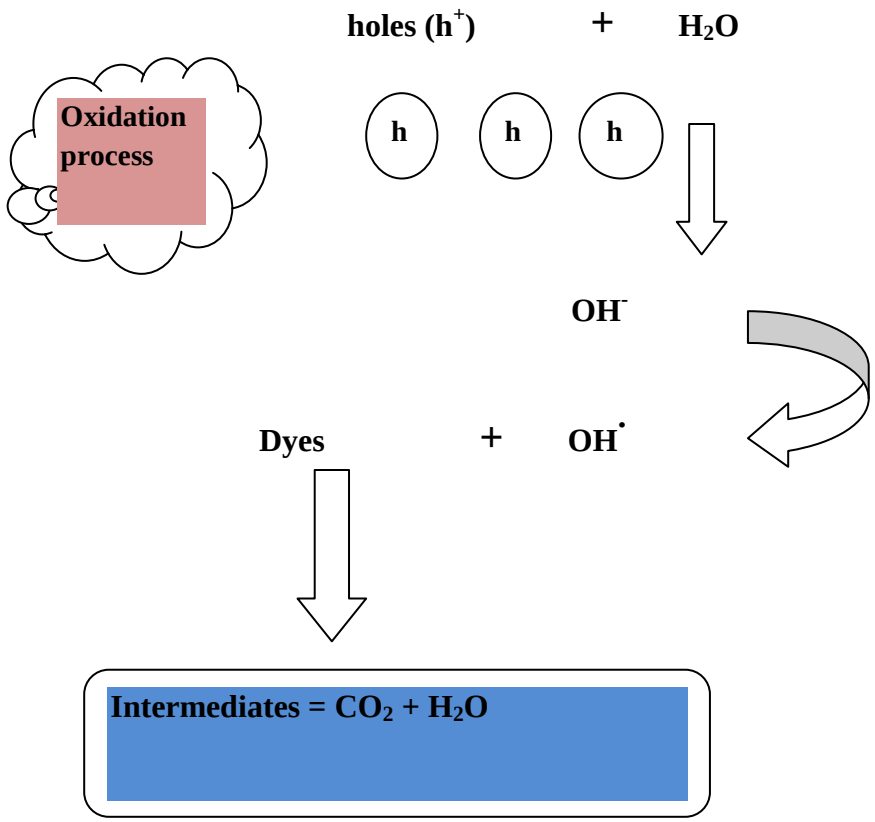

Figure2.2 Schematic representation of oxidation mechanism [31]

In such a case, the organic matter finally decomposes ultimately becoming carbon dioxide and water. Under such circumstances, organic compounds can react straightly with the positive holes, resulting in oxidative decomposition. The complete oxidation processes were shown in figure 2.2

2.2.2 Description of Reduction Mechanism

Figure 2.3 represents the reduction process, the reduction of oxygen contained in the air occurs as a pairing reaction. Reduction of oxygen takes place as an alternative to hydrogen generation due to the fact that oxygen is an easily reducible substance. The conduction band electrons react with dissolved oxygen species to form superoxide anions. These superoxide anions attach to the intermediate products in the oxidative reaction, forming peroxide or changing to hydrogen peroxide and then to water. The reduction is likely to occur more easily in organic matter than in water. Therefore, the higher concentration of organic matter tends to increase the number of positive holes. This reduces the carrier recombination and enhances the photocatalytic activity.

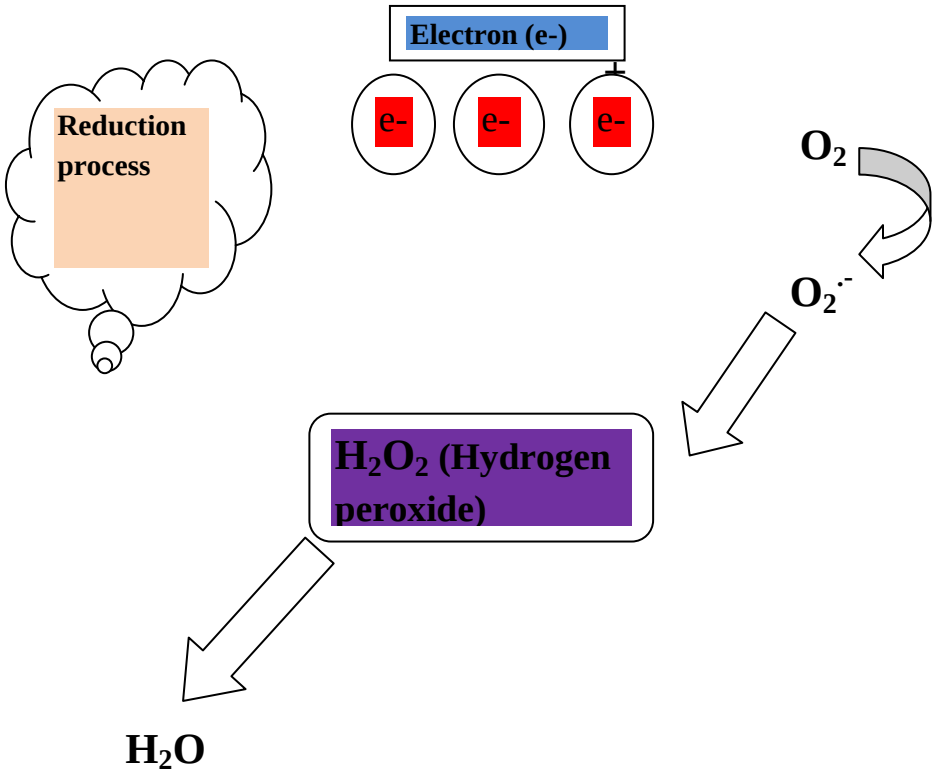

Figure2.3 Schematic representation of reduction mechanism [32]

2.3 Graphitic Carbon Nitride (g-C_3N_4)

2.3.1. Introduction to g-C_3N_4

Graphitic carbon nitride (g-C_3N_4), one of the oldest reported polymers in the literature, has a general formula of (C_3N_3H) n. The history of development could be traced back to 1834 [33].

Research work has been inspired in the1990s due to a theoretical prediction that diamond-like β-g-C_3N_4could have extremely high hardness values. At ambient conditions, g-C_3N_4 is regarded as the most stable allotrope. Similar to graphite, g-$C_3N_4$is a layered material in which van der Waals force holds the stacking layers (covalent C–N bonds) and each layer is composed of tri-s-triazine units connected with planar amino groups. The tri-s-triazine ring structure provides the polymer a high thermal stability (600 ^{O}C in air) and chemical stability both acidic and alkaline environments.

Utilization of g-C_3N_4 in the heterogeneous catalysis is started around a decade ago. The discovery of g-C_3N_4 polymer as a metal-free conjugated semiconductor photocatalysis for water splitting was first reported by Wang et al [34] due to its appealing electronic structure, i.e., having a modulated band gap and being an indirect semiconductor.

Since then these unique properties of g-C_3N_4 make it a promising candidate for visible-light photocatalytic applications utilizing solar energy. Solar energy is attracting worldwide attention by providing about 120,000 TW annually to the earth as one of the green, clean, and sustainable energy resources. Solar-induced chemical processes would be able to greatly extend the applications of g-C_3N_4. Since the landmark discovery of photocatalytic water splitting using TiO_2 electrodes by Fujishima in 1972, photocatalytic technology has been regarded as one of the most important strategies to address global energy and environmental issues. Since then, there have been numerous developments in the fabrication of highly efficient semiconductor-based photocatalysts such as metal-based oxides and sulfides. Notably, g-C_3N_4 has become a new family of next generation, on-toxic, metal-free, earth-abundant, and visible light-driven polymeric semiconductor for applications in the degradation of organic pollutants, hydrogen evolution from water, sensing, imaging, and energy conversion [35].

2.3.2. Synthetic Routes of g-C_3N_4

g-C_3N_4 can be synthesized by directly heating low-cost ingredients like melamine, cyanamide, dicyandiamide and urea, etc. Based on experimental studies and ab initio calculation, a microscopic mechanism of the reaction paths of generatingg-$C_3N_4$from urea or thiourea is shown in figure. Upon heating under a closed air atmosphere, urea first decomposes to ammonia and isocyanic acid and then is converted into some intermediates, such as cyanuric acid, ammelide and ammeline. Cyanuric acid further turns into melamine, which can condense to form melem. Melem undergoes polymerization to melon and further to extended polymers. Finally, polymericg-C_3N_4 is generated from the pyrolysis of precursors [34].

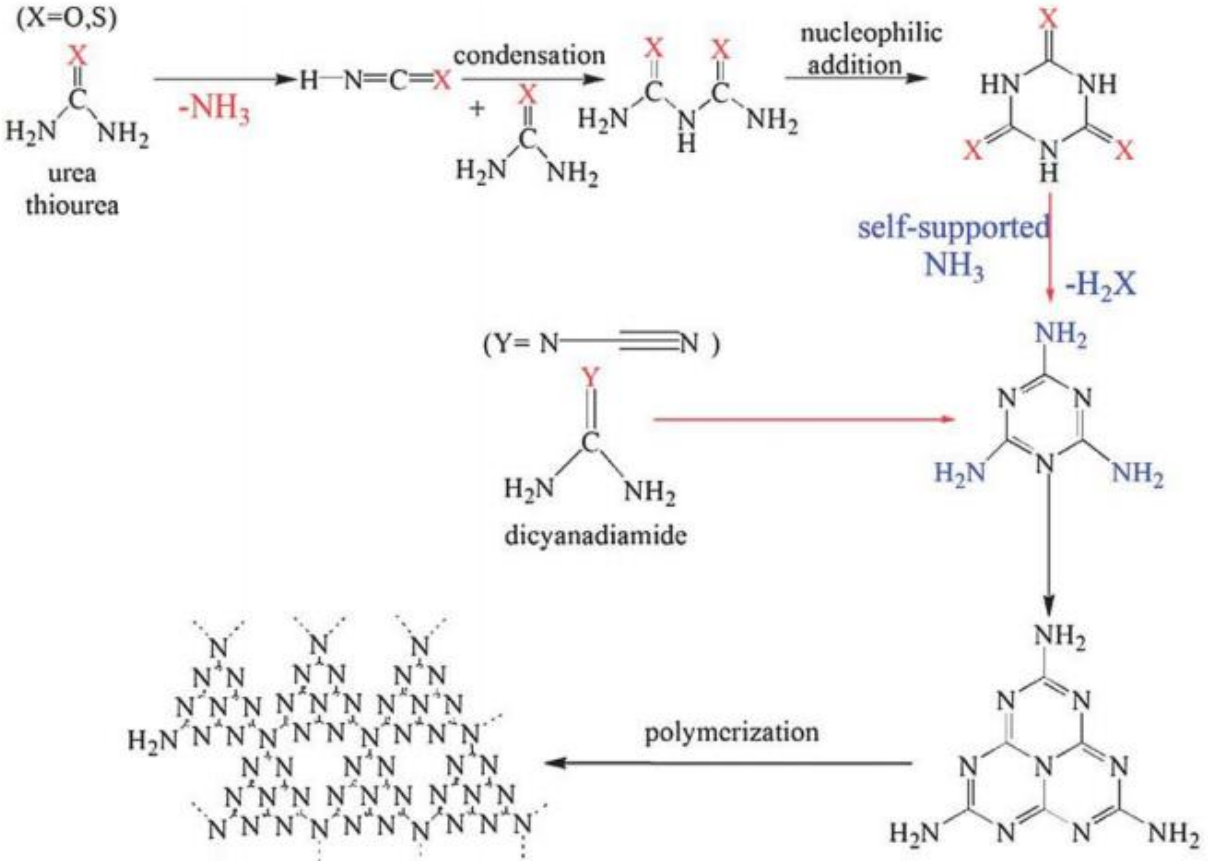

Figure2.4 Microscopic mechanism of the reaction paths of polymeric carbon nitride [36]

2.3.3. Structure and Morphology of g-C_3N_4

g-C_3N_4 has a similarly layered structure to graphite with weak van der Waals forces between layers but a completely different planar structure. The tri-s-triazine (heptazine) rings, relevant to the hypothetical aggregate melem in structure, are shown to be energetically favoured structure for g-C_3N_4. (Figure 2.5) In contrast, to the planar pure covalent bonding of graphite, the planar bonding of g-$C_3N_4$is partially due to hydrogen bonding between strands of polymeric melem units with NH/NH_2 groups

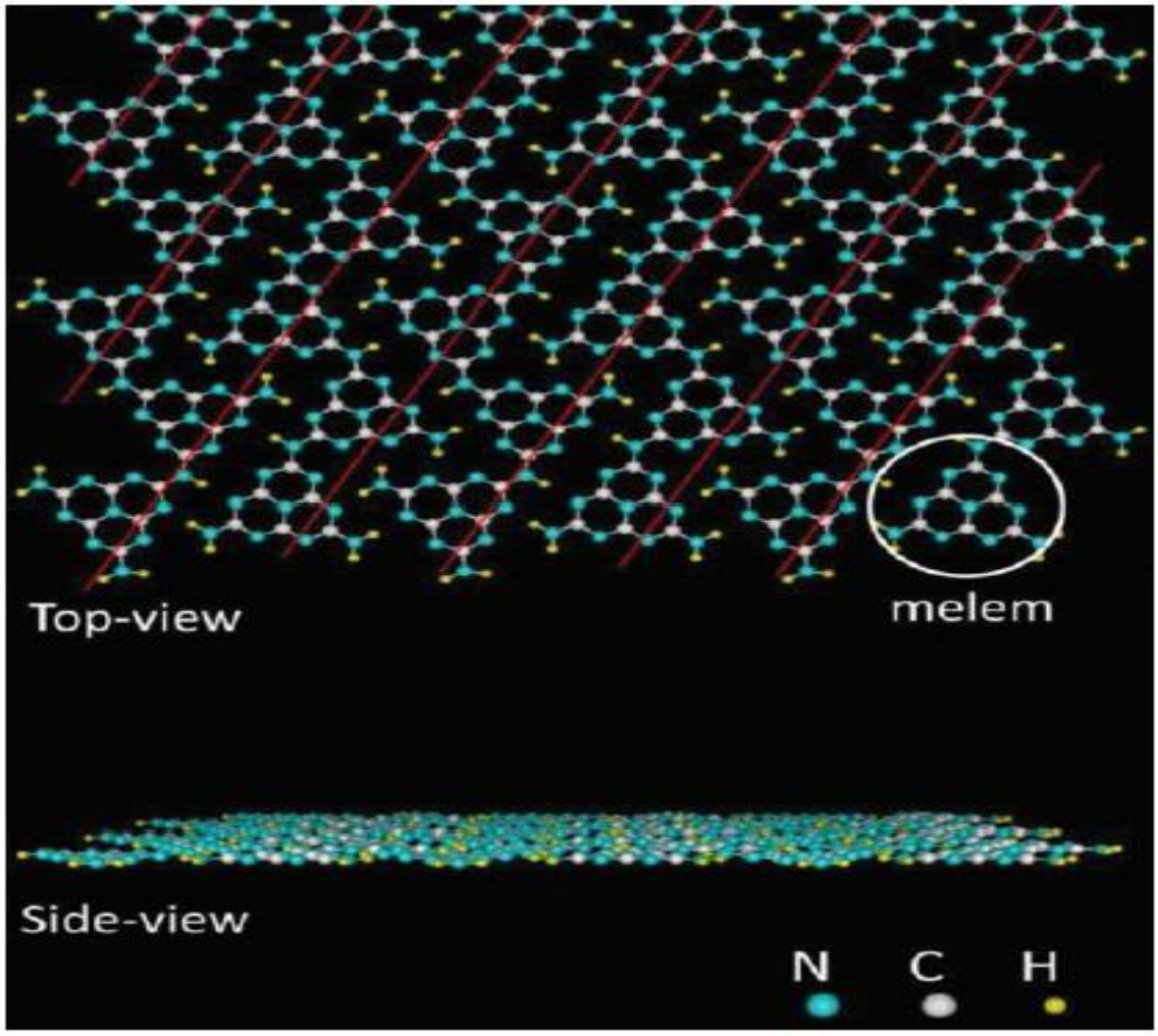

.

Figure2.5 Schematic of monolayer graphitic carbon nitride. N, C and H atoms are represented by light blue, white, and small yellow balls, respectively. The melem unit is marked by the white circle [37].

2.3.4. g-C_3N_4/inorganic semiconductor heterojunction

The semiconductor heterojunction has been an effective architecture to enhance photocatalytic activity by promoting photo generated charge separation. The highest occupied molecular orbital for g-C_3N_4 has been reported to be -1.3 eV versus a normal hydrogen electrode, and it is more negative than the conduction band of conventional wide band gap semiconductors such as TiO_2 and ZnO. This would promote forming a heterostructure with wide band gap semiconductors and to extend their visible light response [38]. Moreover, the combination could not only improve the separation efficiency of electron-hole pairs but could also broaden the absorption band toward the visible region. Therefore, it is no doubt for the trial to build heterojunction between g-C_3N_4 with other inorganic semiconductors. After immobilization on the g-C_3N_4, the problem of agglomeration of inorganic semiconductor e.g. TiO_2 and ZnO have been reported being solved, with further enhancement in the photocatalytic activities [37].

2.4 Cobalt Ferrite Nanoparticles

2.4.1. Spinel Ferrite

Cobalt ferrite nanoparticles have recently become the subject of research interest from the point of view of the synthesis, the structure, the magnetic characterization and the application. Spinel ferrites are also named as cubic ferrites and the chemical formula of spinel ferrites is MFe_2O_4. In the early 21stcentury, the spinel ferrite nanoparticles (MFe_2O_4, in which M represents one or more bivalent transition metals such as Mn, Fe, Co, Ni, Cu, and Zn) have become an important and efficient tool in modern catalytic organic synthesis due to their unique electronic and magnetic properties (easily separate by external magnet), which are quite different from the conventional bulk materials.

In this category (spinel ferrites), cobalt spinel ferrite($CoFe_2O_4$) is an inverse spinel ferrite with all or most Co^{+2} ions occupying octahedral sites (B sites) and the Fe^{+3} ions on both tetrahedral (A sites) and B sites [39]. Cobalt spinel ferrites ($CoFe_2O_4$) have received profound attention due to their high electro-magnetic performance, excellent chemical stability, remarkable mechanical hardness and ferromagnetic behaviors at higher temperature, which are significantly different from their bulk counterparts [40]. Owing to these features, cobalt ferrites have been widely used in sensors, recording devices, magnetic cards, solar cells, magnetic drug delivery, biomedical, catalysis, and biotechnology.

2.4.2. Synthesis of Cobalt Ferrite Nanoparticles

A number of preparation techniques have been explored to synthesize $CoFe_2O_4$ nanoparticles such as micro emulsion [41], sol-gel techniques [42], hydrothermal synthesis [43], solvothermal method [44], co-precipitation [45],electrochemical method [46] ,and combustion methods [47]. Although in most of methods, cobalt ferrite nanoparticles are achieved in the desired or required sizes and microstructures, they are difficult to apply on larger scales due to their expensive and complicated procedures, high reaction temperatures, long reaction times, toxic reagents and by-products, and their potential harm to the environment [48]. Among these, co-precipitation and hydrothermal techniques are easy, versatile, and low-cost methods for the preparation of cobalt ferrite nanoparticles. Co- precipitation is a rapid, easy, and economical process that offers a series of advantages such as controlled crystallite size, high limpidness, no agglomeration of the particles and stable particle surface along with homogeneity [49]. In hydrothermal processes, two factors are very important : optimization of hydrothermal synthetic method and the ion doping or surface modification of cobalt ferrite nanoparticles [50]. Ion doping can lead to structural disorder, change in grain size and lattice strain, and cation redistribution as well as affect the physical and chemical features of cobalt ferrite nanoparticles [50].

2.4.3. Structure of Cobalt Ferrite

The spinel structure is composed of a close-packed oxygen arrangement in which 32 oxygen ions form a unit cell that is the smallest repeating unit in the crystal network. Between the layers of oxygen ions, if we simply visualize them as spheres, there are interstices that may accommodate the metal ions [51]. Generally, if all of these were filled with metal ions, of either 2+ or 3+ valence, the positive charge would be very much greater than the negative charge and so the structure would not be electrically neutral. It turns out that of the 64 tetrahedral sites, only 8 are occupied and out of 32 octahedral sites, only 16 are occupied. In cobalt ferrite, eight units of $CoFe_2O_4$ go into a unit cell of the spinel structure as shown in Figure2.6. In addition to the 32 oxygen ions, there are 16 ferric ions and 8 cobalt ions [52]. Theoretically, the ferric ions preferentially fill the tetrahedral sites, and as there is room for only half of them (eight), the remaining eight go on the octahedral sites as do the eight Co^{++}ions. The anti-ferromagnetic interaction orients these eight Fe^{+++} moments and eight cobalt moments antiparallel to the eight

Fe^{+++}moments on the tetrahedral sites. The Fe^{+++} ion moments will just cancel, but the moments on the cobalt ions give rise to an uncompensated moment or magnetization.

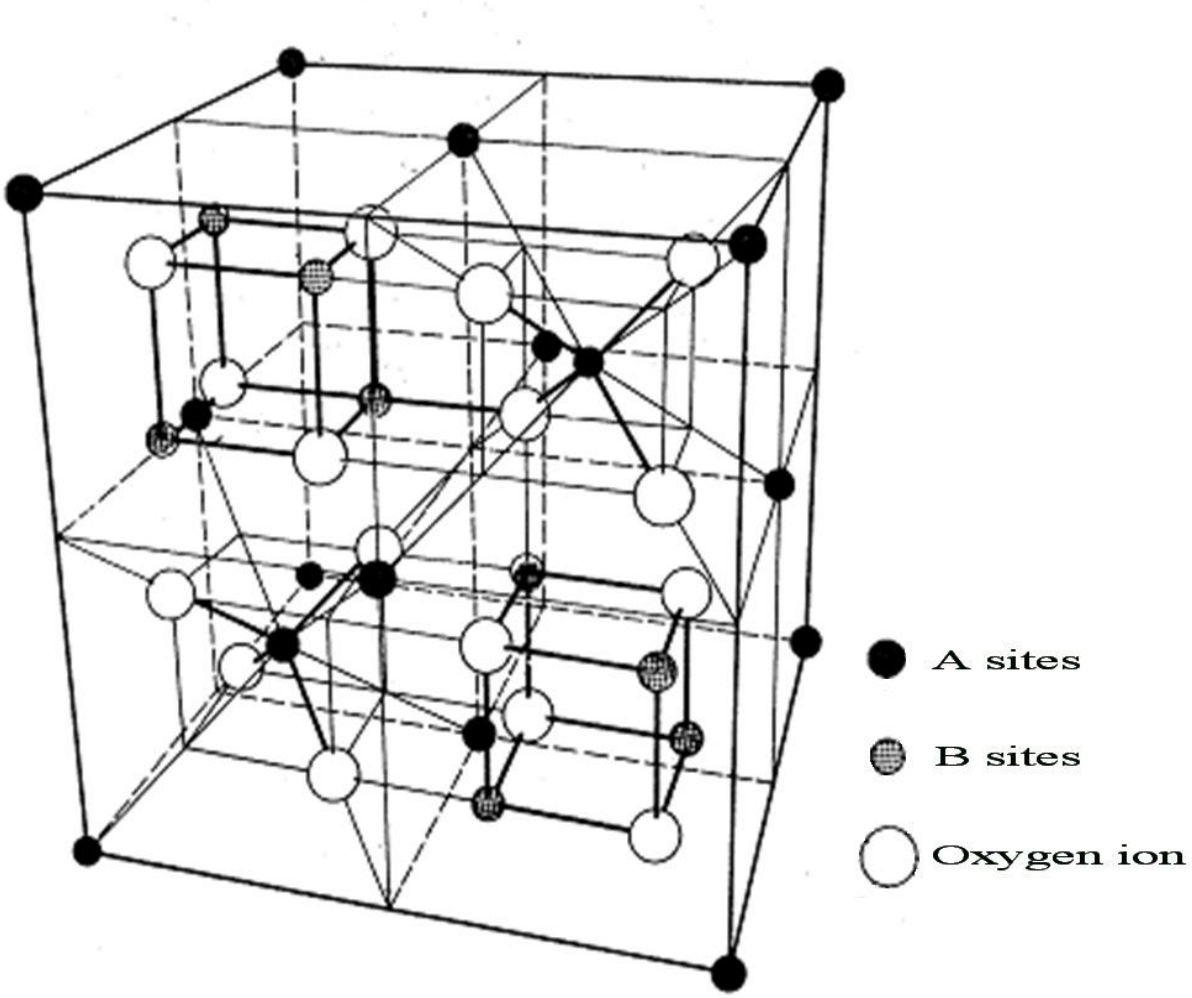

Figure2. 6 Spinel structure [53]

2.5 Applications of Semiconductor Photocatalysis

Photocatalytic material could adsorb or decompose toxic gases in the atmosphere, reducing the adverse effects of toxic gases on the environment. Semiconductor photocatalysis is mild, and the reaction process is relatively simple. In theory, photocatalysis can degrade almost all air pollutants. Therefore, compared with conventional methods such as filtration, adsorption, plasma, and ozone oxidation, photocatalytic technology can completely degrade the pollutants in the air under sunshine, thereby rapidly purifying the air. Photocatalysis is a technology with wide applications and great development potential [54].

.

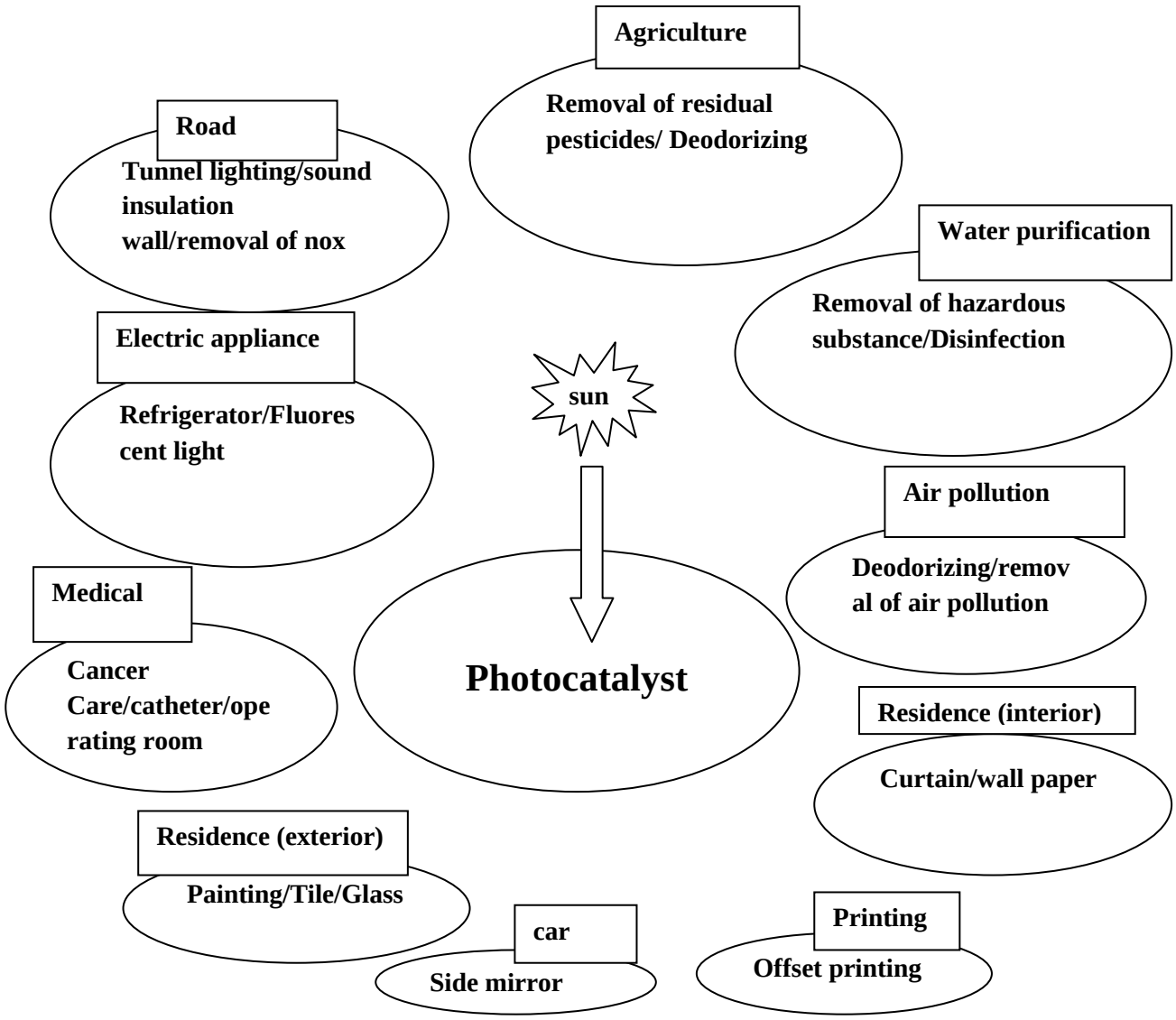

Figure2.7Applications of photocatalysis [55]

2.6 Photocatalytic Mechanism and Influencing Factors

2.6.1. Reaction Mechanism

Photocatalytic reaction is a chemical reaction that takes place under the joint action of light and the photocatalyst. This technology possesses several advantages, including environmental protection, the complete degradation of pollutants, and no secondary pollution [56].

Table 1Effects of influencing factors on photocalaytic reaction[57].

Influencing Factors	Effect on photocatalysis
Catalyst concentration	-The reaction rate increases with the increase of the catalyst concentration. -Above a certain dose, the reaction rate decreases as the catalyst concentration increases.
Light source and light intensity	Light source-provide light of different wavelengths. Light intensity-improve light intensity and promote photocatalytic reaction.
pH value	-Related to target degradation products.
Plus oxidants	-Reducing the recombination of photogenarated electrons and holes and promote photocatalytic efficiency.
Inorganic ion	Anion-improve the separation speed of photogenarated electrons and holes and promote photocatalytic reaction. Becomes a scavenger of hydroxyl radicals, forming anion radicals. Cation-The competitive adsorption of active sites on the surface of the catalyst may affect the photocatalytic degradation of organics.
Temperature	-Has little effect.

Modification Method	Advantage	Disadvantage
Particle doping	-Reduced band gap -Reduced particle size	-Introduce defects
Precious metal depositing	-Enhance electron-hole separation	-Expensive
Surface dye photosensitization	-Broaden the light response range	-Expensive -Dyes may be photolyzed
Semiconductor compound	-reducing the complex of electron-hole pairs -Broaden the light response range	-Energy loss

2.7 Photocatalytic Degradation of Dye

The photocatalytic activities of g-C_3N_4, $CoFe_2O_4$ and different ratios of g-C_3N_4/$CoFe_2O_4$ nanocomposite were evaluated using the photo-degradation of MB solutions under UV–visible light irradiation. Then decrease in the peak intensity of the absorption spectra of the dyes with the increase in irradiation time clearly depicts that the deposited catalysts degrade the dye molecule effectively. The degradation efficiency of prepared catalysts were calculated using the following relation [58].

$$=\frac{Co-C}{Co}\times 100\% = \frac{Ao-A}{Ao}\times 100\%$$

where C_0 is the initial concentration of the tested dyes and C is the concentration of dye solution after the irradiation of UV–visible light at periodic intervals of time. A_0 and A are the corresponding absorption values. It is known that the absorption is proportional to the concentration of the dye solution.

2.8 Methylene Blue (MB)

Dyes are colored organic compounds that are used to impart color to various substrates, including paper, leather, fur, hair, drugs, cosmetics, waxes, greases, plastics, and textile materials [59]. Despite the wide application, most of the dyes are toxic to aquatic life and human. Dye-bearing wastewaters exhibit high chemical and biochemical oxygen demands. The presence of even very low concentrations is cause for polluted the environment. To reduce the negative effects of dye-contaminated wastewater on humans and the environment, the wastewater must be treated carefully before discharge into the main streams. Among these, MB is the most notable dye used for staining in biology, indicator in chemistry and imparting of color for fabrics [60]. Whereas, ingestion of methylene blue through the mouth produces a burning sensation and may cause nausea, vomiting, diarrhea, and gastritis. Once inhaled it can give rise to a short rapid, difficult breathing. Accidental large dose creates chest and abdominal pain, severe headaches, profuse sweating, methemoglobinemia and painful urination [61]. Methylene blue is a basic dye; it has a chemical formula, ($C1_6H_{18}N_3SCl$), its IUPAC name is 3,7-bis(dimethylamino)-phenothiazin-5-ium-chloride with molecular weight 319.85(g/mol) and a λ_{max} wavelength of 664.3 nm [62]. Figure 2.8 shows the chemical structure of methylene blue dye

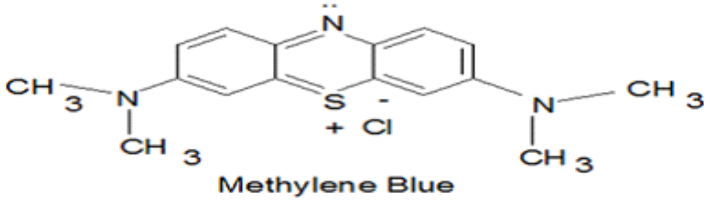

Figure2.8 Chemical structure of methylene blue dye [63]

Methylene blue is soluble in water, and it is an aromatic heterocyclic compound. This means methylene blue is an organic compound that has one or more of the carbon atoms in the backbone of the molecular being replaced with an atom other than carbon. This atom includes nitrogen, oxygen, and sulfur. Methylene blue at room temperature appears as a solid, odorless, dark green powder that turns blue when dissolved in water [64].

CHAPTER THREE

3. MATERIALAND METHOD

3.1 Materials

Chemicals and reagents used for the synthesis of g-C_3N_4/$CoFe_2O_4$ nanocomposite are urea ($(H_2N)_2CO$, 99.8%), Ferric nitrate nonahydrate ($Fe(NO_3)_3.9H_2O$, 98.0%), were obtained from Rajasthan and Newdelhi, India, respectively. Cobaltous nitrate hexahydrate, ($Co(NO_3)_2.6H_2O$ 99%), sodium hydroxide (NaOH 99.8%), and methylene blue ($Cl_6H_{18}N_3SCl$) were obtained from Belgrade, Serbia, Nor bright, China and Sigma Aldrich, China respectively. Besides, the rest of all chemicals used in this study were analytically grade and used without further purification. Distilled water was used throughout the whole experiment.

3.2 Sample Preparation

All plastic containers, crucibles, mortar and pestles were washed thoroughly. Glass was washed with liquid soap, rinsed with dilute water. All stock solution was prepared, autoclaved and stored at recommended temperature till, further use .During sample preparation, dilution and rinsing apparatus prior to analysis.

3.2.1. Synthesis of Graphitic Carbon Nitride (g-C_3N_4)

A facile calcination method was employed to synthesis g-C_3N_4 using urea as a starting material [65]. In a brief, 10 g urea was first dried for 24 h at 80 ^{O}C in a ceramic crucible. The dried urea under aluminum foil was placed in a furnace for calcination at 550 ^{O}C for 3 h. The heating rate of calcination was 2 ^{O}C /min. After cooling, the yellow powder of the synthesized g-C_3N_4 was obtained. The resulting yellow product was collected and ground into powder for further use.

3.2.2. Synthesis of Cobalt ferrite by Co-precipitation Method

Cobalt ferrite nanoparticles were synthesized using the co-precipitation method. In particular, 1.455 g $Co(NO_3)_2$ $6H_2O$ (5mmol) and 4.04 g $Fe(NO_3)_3 \cdot 9H_2O$ (10 mmol) in a 1:2 molar ratio respectively, was used as starting materials. The metal nitrates were dissolved together in a

minimum amount of deionized water to get a clear solution. Deionized distilled water was used as a solvent in order to avoid the production of impurities in the final product. 3M solution of sodium hydroxide was prepared and slowly added to the salt solution drop wise. The pH of the solution was constantly monitored as the NaOH solution was added. The reactants were constantly stirred using a magnetic stirrer until a pH level of 11-12 was reached. The liquid precipitate was then brought to a reaction temperature of 80^{o}C and stirred for one hour. The product was then cooled to room temperature. To get free particles, the precipitate was then washed several times with distilled water and then decanted; the precipitate was dried at 105^{O}C. The acquired substance was then grinded into a fine powder.

3.2.3. The synthesis of g-C_3N_4/ $CoFe_2O_4$Nanocomposites

Samples with different ratios of g-C_3N_4/ $CoFe_2O_4$ were synthesized by a facile co-precipitation method. A typical experiment for the synthesis of g-C_3N_4/ $CoFe_2O_4$ was as follows: 0.1g of the as-prepared g-C_3N_4 powder was dispersed in 100ml deionized distilled water and stirred to form homogenous solution. Then, 0.7275 g $Co(NO_3)_2\ 6H_2O$+2.02 g $Fe(NO_3)_3 9H_2O$ (ratio 1) and 1.455 g $Co(NO_3)_2\ 6H_2O$+ 4.04 g $Fe(NO_3)_3 \cdot 9H_2O$ (ratio 2) in a 1:2 molar ratio was dissolved in 100 mL deionized distilled water.3M (100ml) sodium hydroxide solution was prepared and slowly added to the g-C_3N_4-Co^{2+}& Fe^{3+} salt solution of each ratio drops wise. The liquid precipitate was refluxed using reflux condenser to a reaction temperature of 80^{o}c for 8 hours to complete the formation of nanocomposite and then the product was cooled to room temperature. Finally, the precipitate was washed several times with distilled water and then decanted; the precipitate was dried in oven at 105^{o}c for 5 hours. The acquired substance was then grinded in to a fine powder.

3.3 Characterization Technique

3.3.1. Powder x-ray Diffraction (PXRD)

X-ray diffraction (XRD) is an important and definitive characterization tool widely used to elucidate the structure of synthesized graphitic carbon nitride (g-C_3N_4), cobalt ferrite ($CoFe_2O_4$) and graphitic carbon nitride –cobalt ferrite (g-C_3N_4/$CoFe_2O_4$) composite. Powder diffraction can be used to determine whether a new material such as graphitic nitride, cobalt ferrite has been synthesized, whether a desired graphitic nitride, cobalt ferrite and graphitic carbon nitride-cobalt

ferrite composite has been made or whether a crystallization process has completed. XRD is an integral tool in determining the details structure of a newly synthesized graphitic carbon nitride, cobalt ferrite and graphitic carbon nitride-cobalt ferrite composite. The working principle of XRD is based on applying elastic scattering of X-rays on structure to acquire information on the unit cell parameters of the product. By measuring the angles and intensities of these diffracted X-rays beams. X-ray diffractometer can produce a pictorial view of density of electrons within the crystal [66]. The two-dimensional image can be converted into a three-dimensional model of the density electrons within the crystal using the mathematical method of Fourier transforms.

X-rays are produced when the wavelength of the scattered X-rays interfere constructively. I.e. forming a diffraction pattern. For constructive interference, the difference in the travel path must be equal to integer multiples of the wavelength. When the constructive interference occurs, a diffracted beam of X-rays would leave crystal at the angle equal to that of the incident beam [67]. The general relationship between the wavelengths of incidence X-rays, angles of incidence and spacing between the crystal lattice planes atoms is known as Bragg's law:

$n\lambda=2d\sin\theta$……Equation 3.1

Hence λ =wavelength of x-ray used θ =Angle between incident X-rays and plane of the crystal d= Distance between the planes of the constituent particles in a crystal n= an integer (1, 2, 3...etc.) the diffracted beam makes an angle 2θ. In XRD analysis good sample preparation is extremely important to producing good X-ray diffraction result.

3.3.2. Fourier Transformed Infrared Analysis (FTIR)

Infrared spectroscopy is powerful techniques for the characterization of the as- synthesized graphitic carbon nitride, cobalt ferrite and graphitic carbon nitride-cobalt ferrite composite materials. Most infrared spectrometer measures the absorption of radiation in the mid-infrared region of the electromagnetic spectrum (4000-400cm^{-1}). In this region of the spectrum, absorption is due to many vibrational modes in the sample. Analysis of these vibrational absorption bands provides information the chemical species present. This includes information about the structure of the as-synthesized nanomaterials as well as other functional group. FTIR is used for the analysis of graphitic carbon nitride, cobalt ferrite and its nanocomposite. Herein, FTIR spectra were obtained by using a Bruker ALPHA-P FTIR equipped with an ATR (Attenuated Total Reflection) [68].

3.3.3. Ultraviolet-Visible Spectroscopy (Uv-Vis) Spectroscopy

UV/Vis spectrophotometer is used in the quantitative determination of concentrations of the absorber in the solutions of transition metal ions and highly conjugated organic compounds. The absorption of the samples was recorded in a specific wavelength within the range of 200 and 800 nm using UV-Vis spectrophotometer (752 spectrophotometer).

3.4 Point of Zero Charge (pHpzc) Determination

The pHpzc is defined as the pH of the suspension at which the surface (acidic or basic) functional groups of adsorbents no longer contribute to the pH value of the solution.

The relationship between pHpzc and adsorption capacity is that cation adsorption on any adsorbent will be expected to increase at pH value higher than the pHpzc while anions adsorption will be favorable at pH values lower than pHpzc. It has been reported by earlier researcher that the pHpzc of an adsorbent decreases with increase in acidic groups on the surface of the adsorbents. The effects of pH on the adsorption process may also be explained in terms of pH of the point of zero charge, (pHpzc) at which the surface of adsorbent is neutral [70]. The pH drift method was used to measure the pH at the potential of zero charge (pHpzc) by plotting the change in pH (Y-axis) vs initial pH (X-axis). Then, draw a line where ΔpH (final pH- initial pH) via initial pH. The resulting pH = 0 is taken as the pHpzc [71].

3.5 Photocatalytic Experiment

The photocatalytic studies were performed to investigate g-C_3N_4/$CoFe_2O_4$ nanocomposite performance for the degradation MB. For example, 0.1 g of the photocatalyst was added into 100 mL of 10 mg/L solution of MB. Before photocatalysis, the solution was stirred magnetically for 60 min in the dark to establish an adsorption-desorption equilibrium. Then, the solution was irradiated by tungsten lump (30 W) in the photo reactor.

At a fixed time interval 3 mL of suspension was collected for recording the absorbance at λ_{max}= 664nm a maximum MB. The pH of the solutions was adjusted by adding either 0.1 M HCl or 0.1M NaOH. The degradation (%) was computed by Eq3.2. The photocatalytic performance of g-C_3N_4/$CoFe_2O_4$ was investigated at various contact time, initial concentrations of MB (5, 10, 20, 30 mg/L)), pH (initial – final) of solution and dose of photocatalyst (25mg to 150 mg).

Degradation (%) = $(A_o-A_t)/A_o$* 100 ……. (Eq. 3.2)

CHAPTER FOUR

4. RESULT AND DISCUSION

4.1 Characterization Analysis

4.1.1. Fourier Transformed Infrared Analysis (FTIR)

Fourier transforms infrared spectra (FTIR) were obtained on spectrum 65(PerkinElmer) in the region of 4000–400 cm–^{1} using KBr pellets. FTIR spectroscopy was used to investigate the vibrational functional group present in g-C_3N_4, $CoFe_2O_4$ NPs and g-C_3N_4/$CoFe_2O_4$ nanocomposite photocatalysts. Figure 4.1Shows the FTIR spectra of g-C_3N_4, $CoFe_2O_4$ NPs and g-C_3N_4/$CoFe_2O_4$ nanocomposite sample. The FTIR spectrum of g- C_3N_4 (Figure 4.1a) shows the weak absorption at 808 and 890cm^{-1}is assigned to the bending vibration mode of C-N heterocycles and the characteristic breathing mode of the triazine units [13]. g-C_3N_4 also shows strong bands in the range between 1238– 1640 cm^{-1}, which corresponds to the typical stretching vibration modes of the heptazine heterocyclic ring g-C_3N_4 units [69]. The strong broad band of g-C_3N_4 centered at 3179 cm^{-1} is ascribed to the stretching mode of the N−H bond [70]. Adsorption peak at about 1408 cm^{-1} can be attributed to C–N, and at 1640cm^{-1}due to the C=N stretching mode [71].The stretching vibration modes of N–H and O–H at 3179–3500cm^{-1} [72].

The spectrum of pure $CoFe_2O_4$ NPs (Figure 4.1b) has the distinctive absorption peak at 630 cm^{-1}assigned for the stretching vibration of metal ion (Co-O or Fe-O) in the octahedral and tetrahedral site of the spinel structure [73]. Figure 4.1c, shows the FTIR spectrum of the binary composites of g-C_3N_4/$CoFe_2O_4$. As it is shown in the Figure, the peak due to g-C_3N_4 and $CoFe_2O_4$ NPs are found in the composite. This implies that the presence of both compounds in the composite.

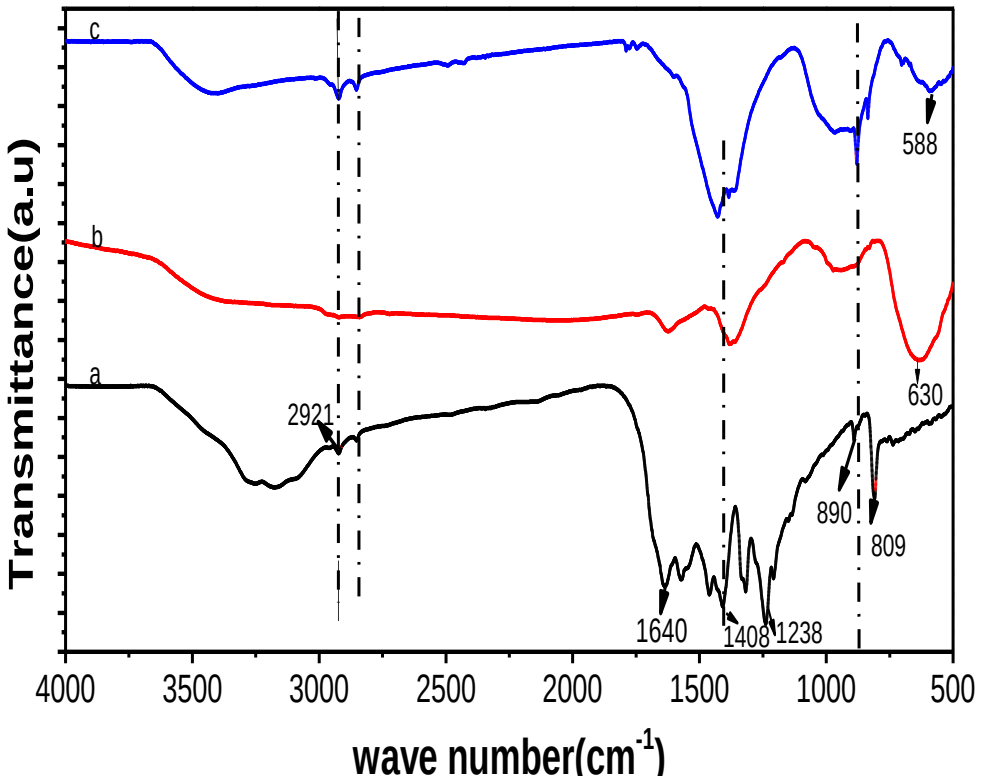

Figure 4. 1 TheFTIR patterns of (a) pure g-C_3N_4 (b) $CoFe_2O_4$ NPs (c) g-C_3N_4/$CoFe_2O$ (ratio 2) nanocomposites

4.1.2. Powder x-ray Diffraction (PXRD) Analysis

The X-ray diffraction (XRD) patterns of the crystal phase was collected using a Bruker D8 diffractometer with Cu-Kα radiation (λ = 1.5418˚A) in the 2Θ range of 10–80^{O}.Figure 4.2 shows the diffraction patterns of the synthesized g-$C_3N_4$from Urea under calcination. The XRD graph shows the formation of peaks at the 2θ value of 13.14^{o} and 27.62^{o},indexed to (100) and (002) planes of graphite-like conjugated triazine aromatic sheets, which matches well with Joint committee on powder diffraction standards (JCPDS) 87–1526 for g-C_3N_4. As a result of indexing, the pattern was assigned to an orthorhombic system having a lattice constant of a ~ 0.7300, b ~ 0.8467 and c ~ 0.6492 nm. The diffraction planes, (100) and (002), are attributed to the pristine interplanar stacking of the conjugated aromatic structure and the interlayer distance of the stacking of g-$C_3N_4$was found to be 0.32 nm at (002) [74]. The average crystallite size for g-C_3N_4calculated using Scherrer relation was found to be 42 nm.

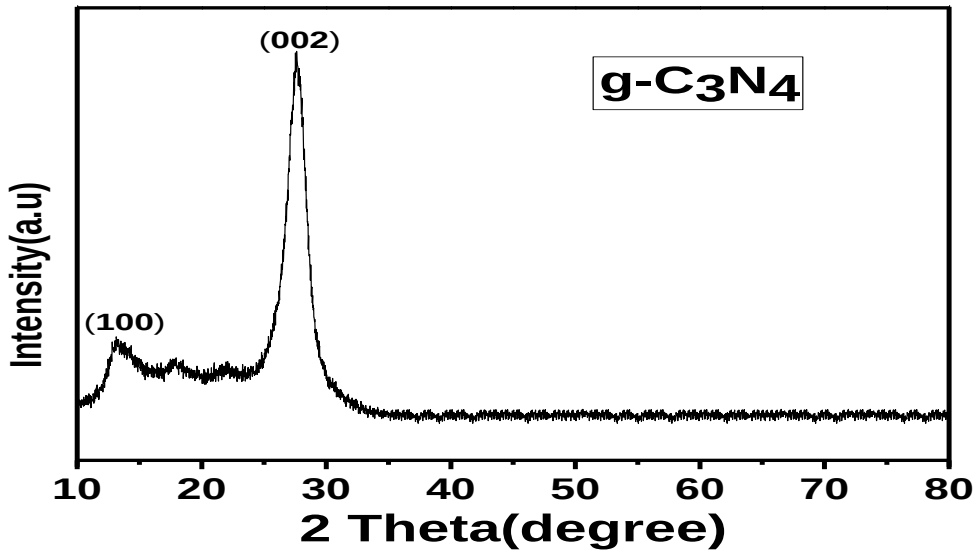

Figure 4. 2 ThePowder XRD pattern of g-C_3N_4 obtained from the calcinations of urea

The phase formation and structural parameters of the synthesized materials were investigated by XRD using Qualx version 2.24 software. The XRD diffractogram of $CoFe_2O_4$ NPs shows high degree of crystallinity (Figure 4.3), have a degree of crystallinity. The diffraction peaks at $2\theta=18.3^o$, 30.1^o, 35.5^o, 37.1^o, 43.1^o, 53.5^o, 57.1^o, 62.6^o, and 74.1^o were indexed to (111), (220), (311), (222), (400), (422), (511), (440), and (533), respectively, of the cubic spinel structure phase of $CoFe_2O_4$ being in agreement with the standard diffraction pattern of $CoFe_2O_4$ (COD: 00-153-3163). In addition, the pattern indicates the formation of pure phase of cobalt ferrite with face centered cubic structure [75]. The crystallite size of particle was calculated to be ~15.73 nm from the full width half maximum of the strongest peak (311) of XRD pattern employing Scherrer's formula.

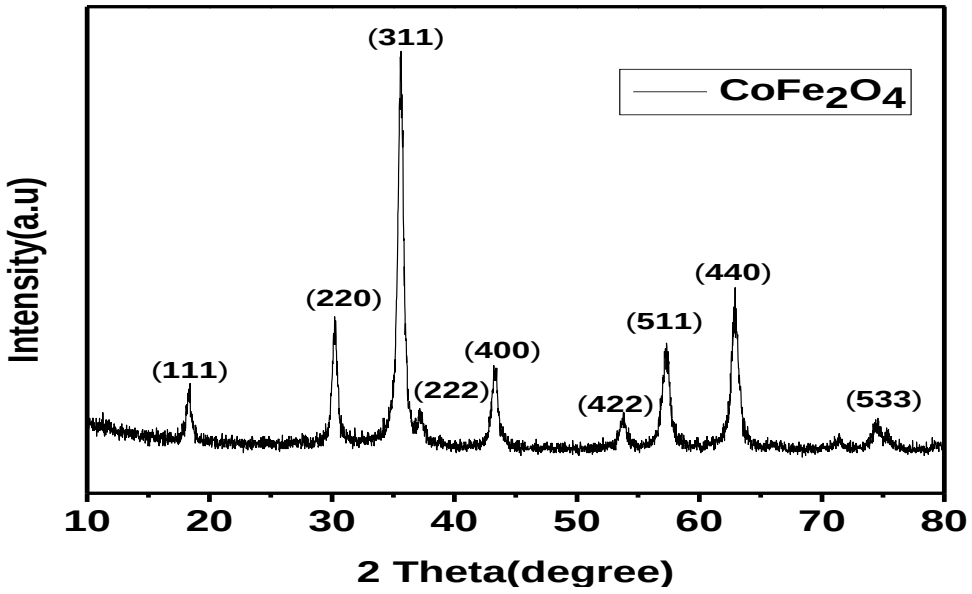

Figure 4. 3 The Powder XRD pattern nanostructured $CoFe_2O_4$NPs synthesized by Co-Precipitation method

The powder XRD profiles of the as- synthesized g-C_3N_4, $CoFe_2O_4$, g-C_3N_4/$CoFe_2O_4$ (ratio 1) and g-C_3N_4/$CoFe_2O_4$ (ratio 2) are presented in Figure 4.4. Figure 4.4a shows the XRD patterns of pure g-C_3N_4. The cubic spinel with pure phase structure of $CoFe_2O_4$ nanoparticles is presented in Figure 4.4b.Whereas; Figure 4.4c and4.4d shows the XRD patterns of g-C_3N_4/$CoFe_2O_4$ (ratio 1) and g-C_3N_4/$CoFe_2O_4$ (ratio 2) nanocomposites respectively. The entire characteristics peak due to the spinel $CoFe_2O_4$ is clearly observed in the composite [76].The diffraction peak due to g-C_3N_4 is not clearly observed in the composite which is due to the small amount of graphite carbon nitride but there is a peak shift, this indicates the formation of composite [77]. The diffraction pattern of g-C_3N_4/$CoFe_2O_4$hetrojunction contained the peak due to both g -C_3N_4 and $CoFe_2O_4$. This confirms that the composite is successfully synthesized through a simple co-precipitation method.

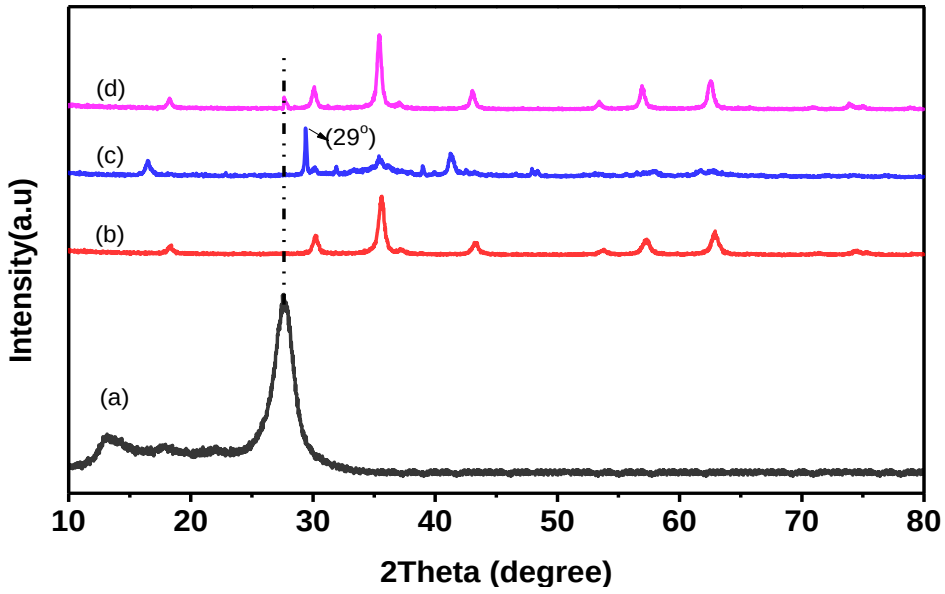

Figure 4. 4 The XRD patterns of (a) pure g-C_3N_4,(b) $CoFe_2O_4$, (c) g-C_3N_4/$CoFe_2O_4$ (ratio 1) and (d) g-C_3N_4/$CoFe_2O_4$(ratio 2)

4.1.3 Surface Charge Analysis

The isoelectric point or Point of Zero Charge (PZC) analysis was used to surface charge of photocatalyst surface as a function of pH, which in turn to investigate the mode of interaction of MB onto photocatalyst surface. The analysis of the pH impact is usually performed based on the pH of point of zero charge (pHpzc) of the photocatalyst. So that, at pH values near pH_{pzc}, the interaction between the pollutants and the photocatalysts surface is very little due to the absence of significant electrostatic forces. However, when the pH of the solution is lower than pH_{pzc}, the photocatalyst surface becomes positively charged and therefore it exerted an electrostatic attraction towards negatively charged compounds. Figure 4.5show the pH of point zero charge analysis of g-C_3N_4/$CoFe_2O_4$ nanocomposite photocatalysts. For the general principle, if the pH is higher than the pH_{pzc}, the surface of the photocatalyst will be charged negatively and therefore it repulses anion compounds. Hence, it could be expected to low removal of at higher pH. At pH values near the pH_{pzc} of the photocatalyst, aggregation of the photocatalyst particles is observed resulting in photocatalyst sedimentation. The pH_{pzc} is the pH at which the adsorbent has a neutral charge on the surface. If pH of the solution is higher than pH_{pzc}, the g-C_3N_4/$CoFe_2O_4$surface becomes negative and attracts cationic dye (MB) from the aqueous solution. The reverse is true for the anionic dye (MO).

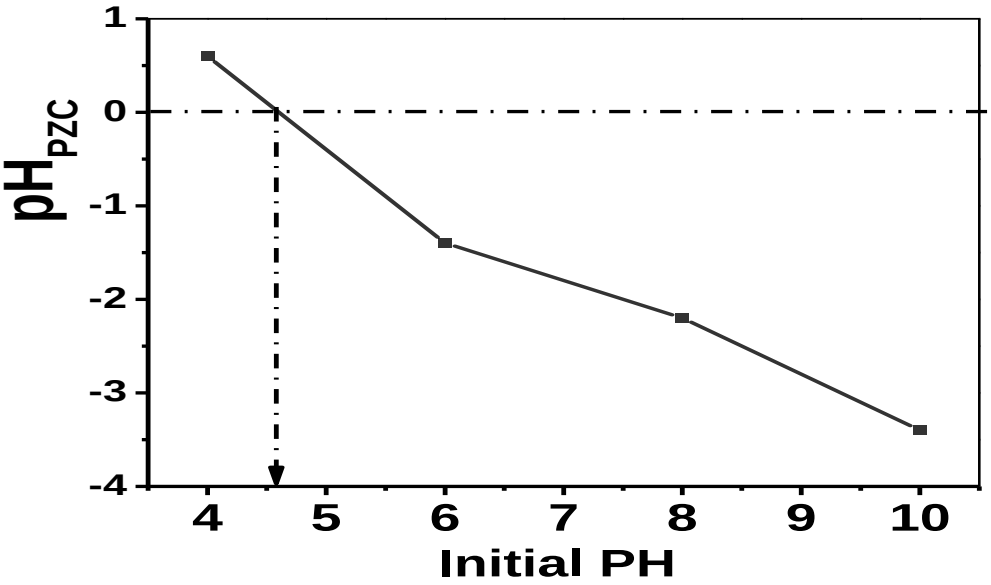

Figure 4. 5 The plot of ΔpH (pH final – pH initial) vs initial pH of solution of g-C_3N_4/$CoFe_2O_4$ nanocomposite (ratio 1)

4.1.3. Photocatalytic degradation of MB Dye

To understand photocatalytic degradation of methylene blue dye using g-C_3N_4/$CoFe_2O_4$(ratio 1) nanocomposite as catalyst, we studied the influence of several factors on the degradation process including contact time, catalyst type, initial concentration of dye, catalyst dose and solution pH.

- **Effect of catalyst type**

Figure 4.6 shows the photocatalytic degradation of different type of photocatalysts. As it is shown in the figure, the g-C_3N_4/$CoFe_2O_4$ (ratio 1) nanocomposite shows the maximum degradation efficiency (97.09 %) than the rest photocatalysts. This is due to the synergistic effect by g-C_3N_4/$CoFe_2O_4$.

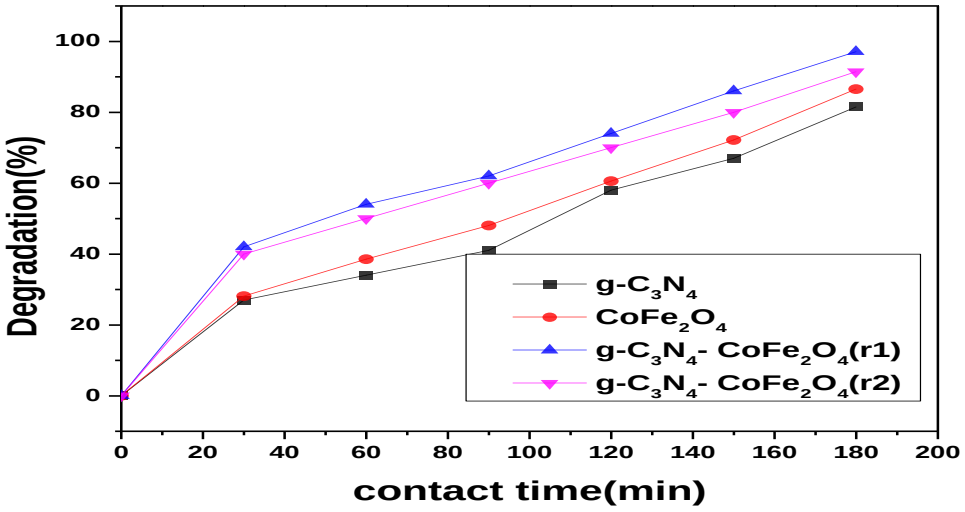

Figure 4. 6 The photocatalytic degradation efficiency (%) of various photocatalysts on MB dye

- **Effect of P^H**

The pH of the medium decides which form of the dye is adsorbed on the surface and how it is degraded [78]. The variation with pH has to be visualized in terms of the surface characteristics of the semiconductor as a fun photocatalytic efficiency of the sample is enhanced. The hole (h^+) oxidizes OH^- formed from the decomposition of water molecules into $^{\cdot}OH$. The hydroxyl radical attacks the MB blue molecules forming CO_2 and H_2O in the action of pH. The impact of pH on MB adsorption by g-C_3-N_4/$CoFe_2O_4$ NPs was investigated by varying the solution pH within the range of 4–10 for a dosage of 50 mg and C_0 of 5 mg/L, conducted at 25 ^{O}C. A 0.1MHCl/NaOH mixture was added to maintain the pH at the required value. As seen in Figure 4.7 the MB removal (%) was enhanced with a rise in solution pH. The pH of the solution was also checked after 24hrs the adsorption process. The pH of the solution changed to approximately its pH_{ZPC} value. At acidic pH, a lower removal was observed due to the competitive interactions of H^+ and catatonic MB, as well as the repulsive force interaction between the dye cations and the positively charged sites. This was confirmed by the stable zeta potential magnitude between pH 4.0 and 8.0 (Figure 4.7). Upon increasing pH (8.0 to 10.0), the MB adsorptive removal increased, due to the increase in the number of negatively charged sites, which led to the existence of an electrostatic force of attraction between the cationic MB and negatively charged sites g-C_3N_4/$CoFe_2O_4$(ratio 1).

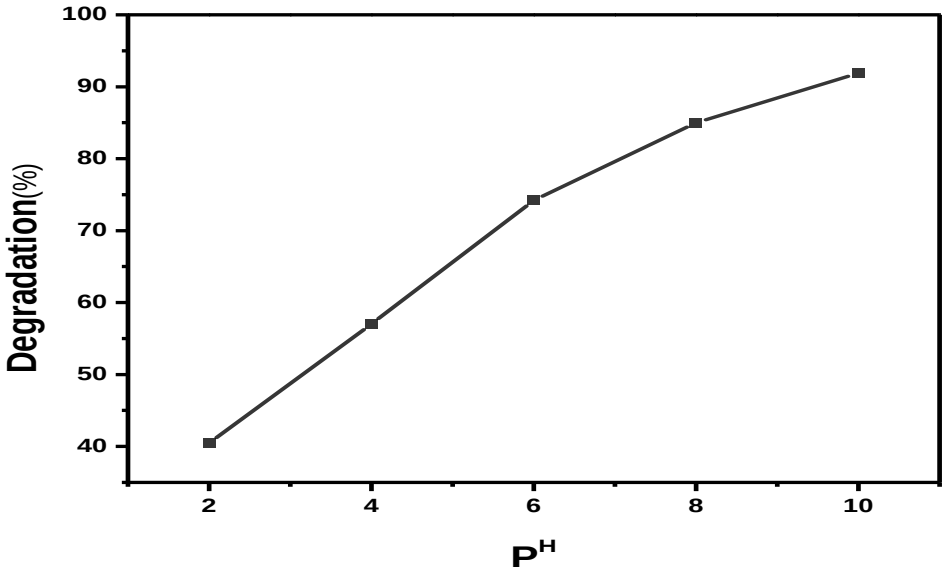

Figure 4. 7 The Effect of pH on the degradation of MB using g-C_3N_4/$CoFe_2O_4$ (ratio 1) nanocomposite

- **Effect of contact time**

Figure 4.8 presents the effect of contact time on the removal of methylene blue using 100 mg of catalysts in aqueous solution. The optimum time for MB degradation was 180 min. Figure 4.8, shows rapid degradation in the initial hour. That is probably due to the larger surface area of the g-C_3N_4/$CoFe_2O_4$ (ratio 1) catalyst being available at beginning for the degradation of MB dye [79]. Maximum degradation efficiency of MB dye was attained by the binary nanocomposite 97.09% within 180 min of contact time. Equilibrium was achieved within this length of time. Figure 4.8 show that the rate of the percentage of MB dye degradation is decrease for further increase time due to the surface adsorption sites become exhausted, the uptake rate is controlled by the rate at which the adsorbate. This result is interesting because equilibrium time is one of the important considerations for economical wastewater treatment applications.

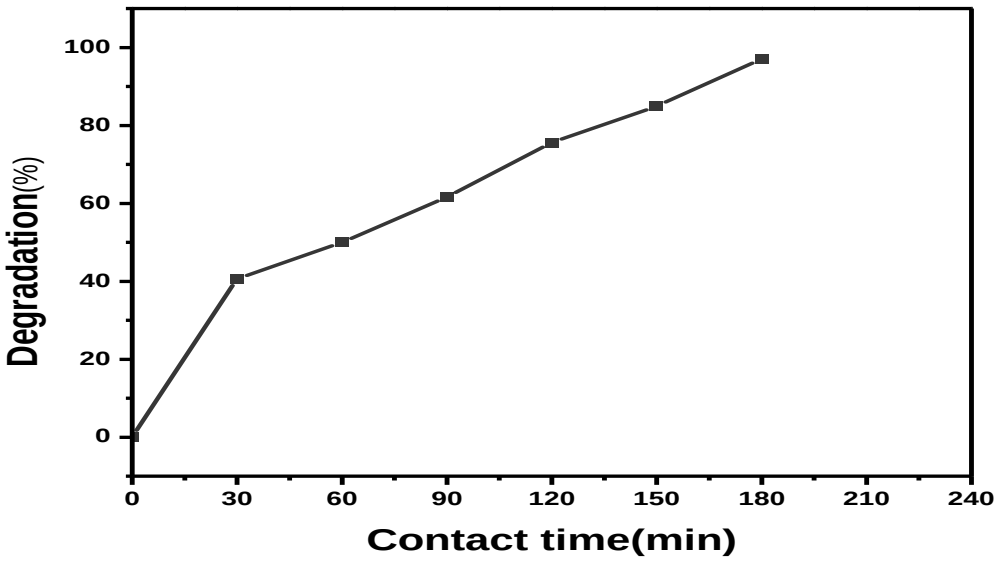

Figure 4. 8 Effect of contact time on the degradation of MB dye (5 mg/L)

- **Effect of Initial concentration MB**

Figure 4.9 shows the effect of initial concentration of MB on the degradation efficiency of g-C_3N_4/$CoFe_2O_4$nanocomposite. In all cases, an initially high rate of adsorption occurred because the MB concentration provided the driving force for the rapid attachment of MB onto the adsorbent surface. As adsorption proceeded, the ratio of MB molecules available adsorption sites decreased, which resulted in a decrease in the adsorption rate until equilibrium was reached. The concentration of MB is an important factor that affects the efficiency and kinetics of degradation. Generally, at low concentrations of contaminants, the rate of degradation increases with the increase of substrate concentration since there are sufficient amounts of radicals and holes for the reaction with contaminants at low substrate concentration. However, beyond the optimal concentration, the removal rate decreases due to the insufficient amount of reactive radicals [80].The adsorption of the dyes on catalyst (g-C_3N_4/$CoFe_2O_4$) was studied by varying the MB concentration (5-30 mg/L).As shown in the Figure, the concentration of MB increases, more reactant molecules are adsorbed on the surface of g-C_3N_4/$CoFe_2O_4$, and as a result reducing the generation of •OH radicals since there are fewer active sites for the adsorption of hydroxyl anions. On the other hand, at higher MB concentrations, the photons are absorbed by the contaminants before they can reach the catalyst surface. Therefore, the absorption of light by the

g-C_3N_4/$CoFe_2O_4$ NPs surface decreases the photocatalytic efficiency. The high concentration of substrate may also cause the deactivation of photocatalyst. Hence the maximum degradation efficiency of MB was found to be 97.09 % at 5 mg/L of MB concentration.

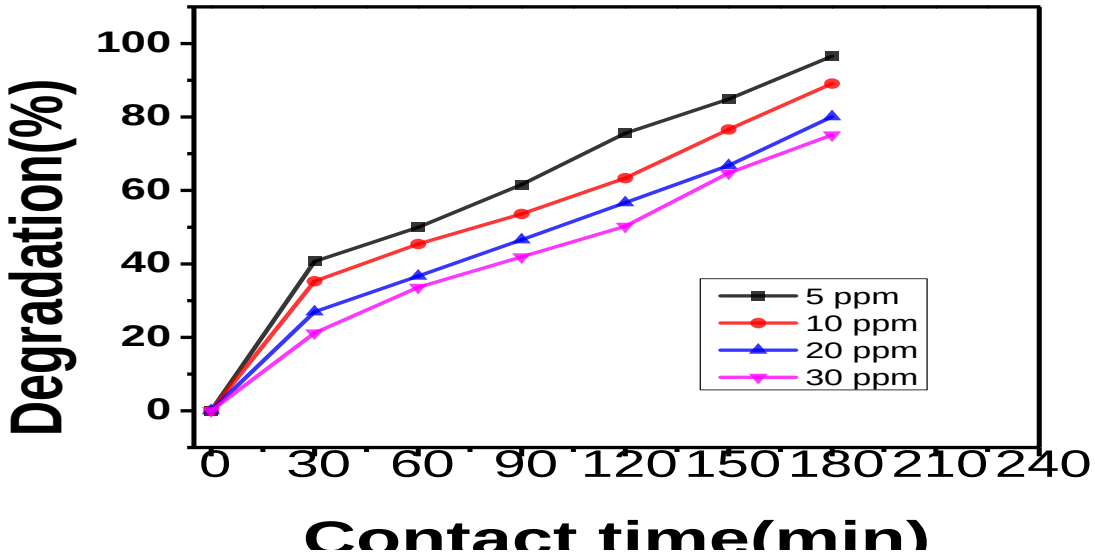

Figure 4. 9 The effect of initial concentration of MB on the degradation of efficiency of g-C_3N_4/ $CoFe_2O_4$ nanocomposite

- **Effect of g-C_3N_4/$CoFe_2O_4$ dose**

Degradation of dye is affected by the amount of the photocatalyst. The degradation percentage of MB dye under visible light irradiation by different amounts of photocatalyst (g-C_3-N_4/$CoFe_2O_4$) were used (25 mg, 50 mg, 100 mg and 150 mg) at a dye concentration of 5 mg/L was examined.. An attempt to enhance MB dye removal was evaluated by examining the effect of adsorbent dosage. As shown in Figure 4.10, it is apparent that the removal percentage of MB dye increases as the adsorbent amount increases, which is the future of heterogeneous photocatalysis. The increase in adsorbent amount actually increases the number of active sites on the photocatalyst surface thus causing an increase in the formation of number of OH radicals which can take part in actual discoloration of dye solution. However, further increase of the photocatalyst dosage resulted in the decrease in removal percentage of MB. This is attributed to the increased turbidity of the suspension, which reduces light penetration and inhibits the photocatalytic process [81].Figure 4.10 shows that the degradation of MB increased from 85.09% – 97.09% with the increase in g-C_3-N_4/$CoFe_2O_4$nanocomposites dosage from 25 to 100 mg. But, further increase in

dosage beyond 100 mg did not show a substantial increasing of MB degradation. Hence, 100 mg of g-C_3N_4/$CoFe_2O_4$ nanocomposites is an optimum amount for the degradation of MB (5 mg/L).

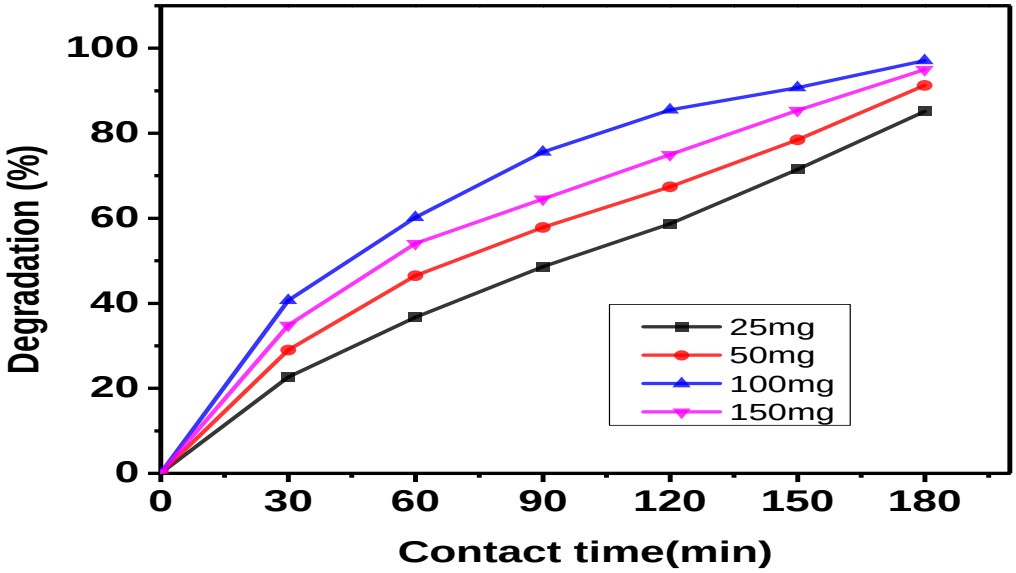

Figure 4. 10 The effect of dosage of g-C_3N_4/$CoFe_2O_4$ (ratio 1) NPs on MB (5 mg/L) degradation.

5. CONCULUSION

In summary, we have successfully synthesized g-C_3N_4, $CoFe_2O_4$ NPs, and different ratios of g-C_3N_4/$CoFe_2O_4$nanocomposites. High yield g-$C_3N_4$was obtained from pyrolysis of Urea in aluminum foil sealed crucible at 550 ^oC for 3 h. A facile co-precipitation $Co^{2+}$and Fe^{3+}salts result the formation of cobalt ferrite nanoparticles with highly crystalline cubic spinel structure.

A simple co-precipitation of cobalt ferrite salts onto g-$C_3N_4$was employed for the synthesis of g-C_3N_4/$CoFe_2O_4$nanocomposite. The effective synthesis of the desired product was investigated by powder XRD and FTIR analysis. The formation of the desired phases of g-$C_3N_4$and its composites validated by XRD investigations.

The pH_{pzc} was done to investigate the surface charge of the composites as a function of pH of the solution. The photocatalytic degradation efficiency of g-C_3N_4/$CoFe_2O_4$nanocomposites was investigated by the degradation of MB. The photocatalytic performances of g-C_3N_4/$CoFe_2O_4$was found to be maximum than pure g-C_3N_4 and $CoFe_2O_4$, this due to the synergetic effect between g-C_3N_4 and $CoFe_2O_4$. The spectra obtained by UV-Vis, and other characterization techniques also revealed that the g-C_3N_4/$CoFe_2O_4$ composite could be easily separated from the solution after reaction, and possessed good visible light response, high chemical stability, and low recombination rates of photo excited charges, which contributed to its high photocatalytic efficiency. This work provides a facile synthesis method to synthesize magnetic composite g-C_3N_4/$CoFe_2O_4$, which is a promising photocatalyst for environmental application.

REFERENCES

1. Sklair, L., *Capitalism and its alternatives*. Vol. 65. 2002: Oxford: Oxford university press.
2. Wittman, H., A. Desmarais, and N. Wiebe, *The origins and potential of food sovereignty.* Food sovereignty: Reconnecting food, nature and community, 2010: p. 1-14.
3. Czekalski, N., E.G. Díez, and H. Bürgmann, *Wastewater as a point source of antibiotic-resistance genes in the sediment of a freshwater lake.* The ISME journal, 2014. **8**(7): p. 1381-1390.
4. Bouwer, H., *Integrated water management for the 21st century: problems and solutions.* Journal of Irrigation and Drainage Engineering, 2002. **128**(4): p. 193-202.
5. Samsami, S., et al., *Recent advances in the treatment of dye-containing wastewater from textile industries: Overview and perspectives.* Process Safety and Environmental Protection, 2020.
6. Teh, C.M. and A.R. Mohamed, *Roles of titanium dioxide and ion-doped titanium dioxide on photocatalytic degradation of organic pollutants (phenolic compounds and dyes) in aqueous solutions: A review.* Journal of Alloys and Compounds, 2011. **509**(5): p. 1648-1660.
7. Khammarnia, S., et al., *Synthesis of FeLaO 3 and FeNdO 3 Magnetic Nanocomposites as Photocatalyst for Organic Dye Removal.* Journal of Cluster Science, 2019. **30**(6): p. 1383-1391.
8. Katheresan, V., J. Kansedo, and S.Y. Lau, *Efficiency of various recent wastewater dye removal methods: a review.* Journal of environmental chemical engineering, 2018. **6**(4): p. 4676-4697.
9. Herrmann, J.-M., *Heterogeneous photocatalysis: fundamentals and applications to the removal of various types of aqueous pollutants.* Catalysis today, 1999. **53**(1): p. 115-129.
10. Xin, G. and Y. Meng, *Pyrolysis synthesized g-C3N4 for photocatalytic degradation of methylene blue.* Journal of Chemistry, 2013. **2013**.
11. Wang, X., et al., *Polymer semiconductors for artificial photosynthesis: hydrogen evolution by mesoporous graphitic carbon nitride with visible light.* Journal of the American Chemical Society, 2009. **131**(5): p. 1680-1681.
12. Yu, G., et al., *Polymer photovoltaic cells: enhanced efficiencies via a network of internal donor-acceptor heterojunctions.* Science, 1995. **270**(5243): p. 1789-1791.
13. Thomas, A., et al., *Graphitic carbon nitride materials: variation of structure and morphology and their use as metal-free catalysts.* Journal of Materials Chemistry, 2008. **18**(41): p. 4893-4908.
14. Wang, L., et al., *In-situ growth of g-C3N4 layer on ZnO nanoparticles with enhanced photocatalytic performances under visible light irradiation.* Materials Letters, 2017. **188**: p. 347-350.
15. Kaur, K., et al., *Photodegradation of organic pollutants using heterojunctions: A review.* Journal of Environmental Chemical Engineering, 2020. **8**(2): p. 103666.
16. Rajiv Gandhi, M., et al., *Graphene and graphene-based composites: a rising star in water purification-A comprehensive overview.* ChemistrySelect, 2016(1): p. 4358-4385.
17. Melendez, A.G., *Structural and dielectric properties of molybdenum doped cobalt ferrite.* 2016.

18. Mousavi, M., A. Habibi-Yangjeh, and S.R. Pouran, *Review on magnetically separable graphitic carbon nitride-based nanocomposites as promising visible-light-driven photocatalysts.* Journal of Materials Science: Materials in Electronics, 2018. **29**(3): p. 1719-1747.
19. Shekofteh-Gohari, M., et al., *Magnetically separable nanocomposites based on ZnO and their applications in photocatalytic processes: A review.* Critical Reviews in Environmental Science and Technology, 2018. **48**(10-12): p. 806-857.
20. Rahman, M.T., *Synthesis, microstructure and performance evaluation of gadolinium incorporated cobalt ferrite ceramics.* 2014.
21. Anusavice, K.J., C. Shen, and H.R. Rawls, *Phillips' science of dental materials*. 2012: Elsevier Health Sciences.
22. Palanivel, B., et al., *Inverse spinel NiFe2O4 deposited g-C3N4 nanosheet for enhanced visible light photocatalytic activity.* Materials Science in Semiconductor Processing, 2019. **100**: p. 87-97.
23. Pillai, S.C., et al., *Photocatalysis as an effective advanced oxidation process.* Advanced oxidation processes for water treatment: fundamentals and applications, 2017: p. 333-381.
24. Anju, A., P. Ravi S, and S. Bechan, *Water pollution with special reference to pesticide contamination in India.* Journal of Water Resource and Protection, 2010. **2010**.
25. Bilal, M., et al., *Biosorption: an interplay between marine algae and potentially toxic elements—a review.* Marine drugs, 2018. **16**(2): p. 65.
26. Serpone, N. and A. Emeline, *Suggested terms and definitions in photocatalysis and radiocatalysis.* International journal of photoenergy, 2002. **4**.
27. Imtiaz, F., J. Rashid, and M. Xu, *Semiconductor Nanocomposites for Visible Light Photocatalysis of Water Pollutants*, in *Concepts of Semiconductor Photocatalysis*. 2019, IntechOpen.
28. Yang, M.Q., et al., *Visible-to-NIR Photon Harvesting: Progressive Engineering of Catalysts for Solar-Powered Environmental Purification and Fuel Production.* Advanced Materials, 2018. **30**(47): p. 1802894.
29. Yu, H., et al., *Smart utilization of carbon dots in semiconductor photocatalysis.* Advanced materials, 2016. **28**(43): p. 9454-9477.
30. Hou, W. and S.B. Cronin, *A review of surface plasmon resonance-enhanced photocatalysis.* Advanced Functional Materials, 2013. **23**(13): p. 1612-1619.
31. Golightly, F., F. Stott, and G. Wood, *The Relationship Between Oxide Grain Morphology and Growth Mechanisms for Fe-Cr-Al and Fe-Cr-Al-Y Alloys.* Journal of the Electrochemical Society, 1979. **126**(6): p. 1035.
32. Roy, K., S. Mukhopadhyay, and H. Mahmoodi-Meimand, *Leakage current mechanisms and leakage reduction techniques in deep-submicrometer CMOS circuits.* Proceedings of the IEEE, 2003. **91**(2): p. 305-327.
33. Lotsch, B.V., *From molecular building blocks to condensed carbon nitride networks: structure and reactivity*. 2006, lmu.
34. Ong, W.-J., et al., *Graphitic carbon nitride (g-C3N4)-based photocatalysts for artificial photosynthesis and environmental remediation: are we a step closer to achieving sustainability?* Chemical reviews, 2016. **116**(12): p. 7159-7329.

35. Wang, A., et al., *Recent advances of graphitic carbon nitride-based structures and applications in catalyst, sensing, imaging, and LEDs.* Nano-micro letters, 2017. **9**(4): p. 1-21.
36. Zhang, Y., et al., *Porous graphitic carbon nitride synthesized via direct polymerization of urea for efficient sunlight-driven photocatalytic hydrogen production.* Nanoscale, 2012. **4**(17): p. 5300-5303.
37. Kang, Y., et al., *An amorphous carbon nitride photocatalyst with greatly extended visible-light-responsive range for photocatalytic hydrogen generation.* Advanced materials, 2015. **27**(31): p. 4572-4577.
38. Jiang, Y., et al., *Enhancement of photocatalytic hydrogen evolution activity of porous oxygen doped g-C3N4 with nitrogen defects induced by changing electron transition.* Applied Catalysis B: Environmental, 2019. **240**: p. 30-38.
39. Chaibakhsh, N. and Z. Moradi-Shoeili, *Enzyme mimetic activities of spinel substituted nanoferrites (MFe2O4): A review of synthesis, mechanism and potential applications.* Materials Science and Engineering: C, 2019. **99**: p. 1424-1447.
40. Pervin, K., *Investigation of structural, photocatalytic and magnetic properties of dy doped cofe2o4 nanoparticles prepared by hydrothermal method.* 2018.
41. Cote, L.J., et al., *Continuous hydrothermal synthesis of CoFe2O4 nanoparticles.* Fluid Phase Equilibria, 2003. **210**(2): p. 307-317.
42. Larbot, A., et al., *Inorganic membranes obtained by sol-gel techniques.* Journal of Membrane Science, 1988. **39**(3): p. 203-212.
43. Feng, S. and R. Xu, *New materials in hydrothermal synthesis.* Accounts of chemical research, 2001. **34**(3): p. 239-247.
44. Sun, C., et al., *Controlled synthesis of CeO2 nanorods by a solvothermal method.* Nanotechnology, 2005. **16**(9): p. 1454.
45. Doerner, H.A. and W.M. Hoskins, *Co-Precipitation of radium and barium sulfates1*. Journal of the American Chemical Society, 1925. **47**(3): p. 662-675.
46. Hodges, A.M., et al., *Electrochemical method*. 1999, Google Patents.
47. Weinberg, F.J., *Advanced combustion methods*. 1986, Imperial College of Science and Technology, London.
48. Hajalilou, A. and S.A. Mazlan, *A review on preparation techniques for synthesis of nanocrystalline soft magnetic ferrites and investigation on the effects of microstructure features on magnetic properties.* Applied Physics A, 2016. **122**(7): p. 680.
49. Kazemi, M., M. Ghobadi, and A. Mirzaie, *Cobalt ferrite nanoparticles (CoFe2O4 MNPs) as catalyst and support: magnetically recoverable nanocatalysts in organic synthesis.* Nanotechnology Reviews, 2018. **7**(1): p. 43-68.
50. Wu, X., et al., *Effect of the rare-earth substitution on the structural, magnetic and adsorption properties in cobalt ferrite nanoparticles.* Ceramics International, 2016. **42**(3): p. 4246-4255.
51. Goldman, A., *Crystal structure of ferrites*, in *Handbook of Modern Ferromagnetic Materials*. 1999, Springer. p. 207-227.
52. Mahiuddin Talukder, M., *Investigation on electrical and magnetic properties of Mn0. 50Zn0. 50-xCUxFe2O4 ferrites.* 2011.
53. Hill, R.J., J.R. Craig, and G. Gibbs, *Systematics of the spinel structure type.* Physics and chemistry of minerals, 1979. **4**(4): p. 317-339.

54. Pelaez, M., et al., *A review on the visible light active titanium dioxide photocatalysts for environmental applications.* Applied Catalysis B: Environmental, 2012. **125**: p. 331-349.
55. Wang, R., et al., *Recent progress in carbon quantum dots: synthesis, properties and applications in photocatalysis.* Journal of Materials Chemistry A, 2017. **5**(8): p. 3717-3734.
56. Leson, G. and A.M. Winer, *Biofiltration: an innovative air pollution control technology for VOC emissions.* Journal of the Air & Waste Management Association, 1991. **41**(8): p. 1045-1054.
57. Wen, X.-J., et al., *Photocatalytic degradation of ciprofloxacin by a novel Z-scheme CeO2–Ag/AgBr photocatalyst: Influencing factors, possible degradation pathways, and mechanism insight.* Journal of catalysis, 2018. **358**: p. 141-154.
58. Kumar, A., et al., *Biochar-templated g-C3N4/Bi2O2CO3/CoFe2O4 nano-assembly for visible and solar assisted photo-degradation of paraquat, nitrophenol reduction and CO2 conversion.* Chemical Engineering Journal, 2018. **339**: p. 393-410.
59. Gonawala, K.H. and M.J. Mehta, *Removal of color from different dye wastewater by using ferric oxide as an adsorbent.* Int J Eng Res Appl, 2014. **4**(5): p. 102-109.
60. Sulugambari, Z.B., *Bioremediation of Local Textile Wastewater Using Indigenous Bacteria Isolated from Soil Contaminated with Dye Effluent*. 2018, Kwara State University (Nigeria).
61. Puvaneswari, N., J. Muthukrishnan, and P. Gunasekaran, *Toxicity assessment and microbial degradation of azo dyes.* 2006.
62. Garg, V.K., et al., *Basic dye (methylene blue) removal from simulated wastewater by adsorption using Indian Rosewood sawdust: a timber industry waste.* Dyes and pigments, 2004. **63**(3): p. 243-250.
63. Wainwright, M. and K.B. Crossley, *Methylene blue-a therapeutic dye for all seasons?* Journal of chemotherapy, 2002. **14**(5): p. 431-443.
64. Nguyen, T.B., et al., *Activation of persulfate by CoO nanoparticles loaded on 3D mesoporous carbon nitride (CoO@ meso-CN) for the degradation of methylene blue (MB).* Science of The Total Environment, 2019. **675**: p. 531-541.
65. Lan, Z.-A., G. Zhang, and X. Wang, *A facile synthesis of Br-modified g-C3N4 semiconductors for photoredox water splitting.* Applied Catalysis B: Environmental, 2016. **192**: p. 116-125.
66. Bunaciu, A.A., E.G. UdriŞTioiu, and H.Y. Aboul-Enein, *X-ray diffraction: instrumentation and applications.* Critical reviews in analytical chemistry, 2015. **45**(4): p. 289-299.
67. Jüstel, D., G. Friesecke, and R.D. James, *Bragg–von Laue diffraction generalized to twisted X-rays.* Acta Crystallographica Section A: Foundations and Advances, 2016. **72**(2): p. 190-196.
68. Wang, L. and B. Mizaikoff, *Application of multivariate data-analysis techniques to biomedical diagnostics based on mid-infrared spectroscopy.* Analytical and bioanalytical chemistry, 2008. **391**(5): p. 1641-1654.
69. Papailias, I., et al., *Effect of processing temperature on structure and photocatalytic properties of g-C3N4.* Applied Surface Science, 2015. **358**: p. 278-286.
70. Wei, K., et al., *One-step fabrication of g-C3N4 nanosheets/TiO2 hollow microspheres heterojunctions with atomic level hybridization and their application in the multi-*

component synergistic photocatalytic systems. Applied Catalysis B: Environmental, 2018. **222**: p. 88-98.
71. Li, X., et al., *Preparation and characterization of graphitic carbon nitride through pyrolysis of melamine.* Applied Physics A, 2009. **94**(2): p. 387-392.
72. Yan, S., Z. Li, and Z. Zou, *Photodegradation performance of g-C3N4 fabricated by directly heating melamine.* Langmuir, 2009. **25**(17): p. 10397-10401.
73. Amaliya, A.P., S. Anand, and S. Pauline, *Investigation on structural, electrical and magnetic properties of titanium substituted cobalt ferrite nanocrystallites.* Journal of Magnetism and Magnetic Materials, 2018. **467**: p. 14-28.
74. Yu, Z., et al., *Nature-mimic method to fabricate polydopamine/graphitic carbon nitride for enhancing photocatalytic degradation performance.* ACS Sustainable Chemistry & Engineering, 2017. **5**(9): p. 7840-7850.
75. Maaz, K., et al., *Synthesis and magnetic properties of cobalt ferrite (CoFe2O4) nanoparticles prepared by wet chemical route.* Journal of magnetism and magnetic materials, 2007. **308**(2): p. 289-295.
76. Saha, M., S. Mukherjee, and A. Gayen, *Microstructure, optical and magnetic properties of inverse spinel CoFe2O4 synthesized by microemulsion process assisted by CTAB and AOT.* Aust Ceram Soc, 2016. **52**: p. 150-162.
77. Natarajan, T.S. and R.J. Tayade, *Photocatalysis: Present, past and future.* Inorganic Pollutants in Wastewater: Methods of Analysis, Removal and Treatment, 2017. **16**: p. 1.
78. Palanivel, B., et al., *rGO supported g-C3N4/CoFe2O4 heterojunction: Visible-light-active photocatalyst for effective utilization of H2O2 to organic pollutant degradation and OH radicals production.* Journal of Environmental Chemical Engineering, 2020: p. 104698.
79. Sarioglu, M. and U. Atay, *Removal of methylene blue by using biosolid.* Global Nest J, 2006. **8**(2): p. 113-120.
80. Singh, J., et al., *Potential degradation of methylene blue (MB) by nano-metallic particles: A kinetic study and possible mechanism of MB degradation.* Environmental Engineering Research, 2017. **23**(1): p. 1-9.
81. Akpan, U.G. and B.H. Hameed, *Parameters affecting the photocatalytic degradation of dyes using TiO2-based photocatalysts: a review.* Journal of hazardous materials, 2009. **170**(2-3): p. 520-529.